The Tropospheric Response to Tropical and Subtropical Zonally Asymmetric Torques: Analytical and Idealized Numerical Model Results

TIFFANY A. SHAW

Department of Earth and Environmental Sciences, and Department of Applied Physics and Applied Mathematics, Columbia University, New York, New York

WILLIAM R. BOOS

Department of Geology and Geophysics, Yale University, New Haven, Connecticut

(Manuscript received 16 May 2011, in final form 3 August 2011)

ABSTRACT

The tropospheric response to prescribed tropical and subtropical zonally asymmetric torques, which can be considered as idealizations of vertical momentum transfers by orographic gravity waves or convection, is investigated. The linear analytical Gill model response to westward upper-tropospheric torques is compared to the response to a midtropospheric heating, which is a familiar point of reference. The response to an equatorial torque projects onto a Kelvin wave response to the east that is of opposite sign to the response to the east of the heating at upper levels. In contrast, the torque and heating both produce Rossby gyres of the same sign to the west of the forcing and the zonal-mean streamfunction responses are identical. When the forcings are shifted into the Northern Hemisphere, the streamfunction responses have opposite signs: there is upwelling in the Southern (Northern) Hemisphere in response to the torque (heating).

The nonlinear response to westward torques was explored in idealized general circulation model experiments. In the absence of a large-scale meridional temperature gradient, the response to an equatorial torque was confined to the tropics and was qualitatively similar to the linear solutions. When the torque was moved into the subtropics, the vorticity budget response was similar to a downward control–type balance in the zonal mean. In the presence of a meridional temperature gradient, the response to an equatorial torque involved a poleward shift of the midlatitude tropospheric jet and Ferrel cell. The response in midlatitudes was associated with a poleward shift of the regions of horizontal eddy momentum flux convergence, which coincided with a shift in the upper-tropospheric critical line for baroclinic waves. The shift in the critical line was caused (in part) by the zonal wind response to the prescribed torque, suggesting a possible cause of the response in midlatitudes. Overall, this hierarchy of analytical and numerical results highlights robust aspects of the response to tropical and subtropical zonally asymmetric torques and represents the first step toward understanding the response in fully comprehensive general circulation models.

1. Introduction

Momentum transfers by disturbances to the zonal mean play an important role in the general circulation of the atmosphere across a wide range of spatial scales. Horizontal eddy momentum flux convergences associated with baroclinic waves contribute to the Ferrel cell and shape the structure of the jet streams and surface winds in the midlatitude troposphere (Held 2000). Likewise, the convergence of Eliassen–Palm fluxes associated with both baroclinic and planetary scale waves drive the Brewer–Dobson circulation in the stratosphere (Andrews et al. 1987). Both of these examples involve horizontal momentum transfers by waves that are resolved in global climate models. In contrast, important vertical eddy momentum flux convergences are associated with processes that take place on spatial scales that are unresolved in global climate models. As a result such transfers must be parameterized. These transfers also play an important role in the atmospheric general circulation.

It is well established that the vertical momentum transfer by internal gravity waves forced by topography,

Corresponding author address: Dr. Tiffany A. Shaw, Department of Earth and Environmental Sciences, and Department of Applied Physics and Applied Mathematics, Columbia University, P.O. Box 1000, 61 Route 9W, Palisades, NY 10964.
E-mail: tas2163@columbia.edu

DOI: 10.1175/JAS-D-11-0139.1

© 2012 American Meteorological Society

called orographic gravity wave drag (OGWD), plays a crucial role in the modeled general circulation. The inclusion of OGWD in a general circulation model reduces the zonal wind in a region extending from the surface topography to the lower stratosphere, warms the Arctic troposphere, and also brings the surface wind distribution and sea level pressure pattern closer to observations during Northern Hemisphere (NH) winter (Palmer et al. 1986; McFarlane 1987; Stephenson 1994). The zonal-mean impacts of OGWD on the general circulation are typically explained using the theory of downward control (Haynes et al. 1991), which assumes a zonal-mean balance between the Coriolis force and the OGWD. However, the role of tropospheric eddies in modulating the downward-control response has been recognized recently (Song and Robinson 2004; Chen and Zurita-Gotor 2008).

Vertical momentum transfer by convection, called convective momentum transfer (CMT), has been estimated in field campaigns and shown to be significant (LeMone 1983; LeMone et al. 1984). It has also been estimated as a residual in the tropical momentum budget using reanalysis data (Carr and Bretherton 2001; Lin et al. 2004). Several CMT parameterizations have been developed (Schneider and Lindzen 1976; Zhang and Cho 1991; Gregory et al. 1997) and the parameterized momentum transfers occur deep within the tropics and extend into the midlatitudes (see Fig. 1 in Richter and Rasch 2008). Several studies have shown that including such transfers in a general circulation model improves the modeled Hadley circulation (both the upper and lower branches) and the zonal wind at the surface and in the tropical troposphere (Zhang and McFarlane 1995; Wu et al. 2003, 2007; Richter and Rasch 2008). The zonal-mean impacts of CMT were considered by Song et al. (2008).

The atmospheric response to momentum transfers has generally been studied in idealized contexts by considering the response to prescribed zonally symmetric torques in the midlatitudes (Eliassen 1951; Haynes et al. 1991; Shepherd et al. 1996; Song and Robinson 2004; Ring and Plumb 2007; Chen and Zurita-Gotor 2008). When the torque is applied in the midlatitudes above the tropopause, it results in a well-known downward control response with the applied torque balanced by the Coriolis torque (Haynes et al. 1991) in the steady-state limit. This balance leads to a mean meridional circulation that extends from the region of the applied torque to the surface. Below the tropopause tropospheric eddies can modulate the response (Song and Robinson 2004; Chen and Zurita-Gotor 2008). While zonally symmetric torques are a reasonable approximation for understanding the atmospheric response to momentum transfers by large-scale waves, they are not appropriate when studying the atmospheric response to vertical momentum transfers associated with submesoscale processes such as orographic gravity waves and convection. These processes are inherently zonally asymmetric and as such the atmospheric response to the associated torques is likely different from that obtained in classical downward control theory. Furthermore, the torques associated with OGWD and CMT occur mainly in low latitudes (from the deep tropics to the subtropics). The tropospheric response to a zonally asymmetric torque in low latitudes has received much less attention.

In contrast, in the tropical atmosphere, much of the focus has been on the atmospheric response to a zonally asymmetric diabatic heating. The impacts of momentum transfers in the tropical and subtropical upper troposphere have not been extensively studied even though several recent studies have highlighted the impact on the Hadley circulation of baroclinic eddy momentum fluxes in these regions (Walker and Schneider 2006; Schneider and Bordoni 2008; Bordoni and Schneider 2008).

Here we investigate the tropospheric response to a prescribed zonally asymmetric torque in the tropics and subtropics. We begin with an analysis of the response in the analytical Gill (1980) model. The linear analytical response is compared to the well-known response to a prescribed diabatic heating; we choose the heating as a well-known point of reference. The response is subsequently compared to idealized nonlinear simulations of a dry primitive equations model in the absence of a large-scale meridional temperature gradient. The torque is moved from the tropics to the subtropics in order to mimic the varied locations of torques associated with parameterized OGWD and CMT. Finally, we examine how baroclinic eddies modify the response to the prescribed tropical and subtropical torques. Because this is an idealized study in which we take the approach of examining how the response to a given torque changes as a function of that torque's latitude, our forcings may have amplitudes that are realistic at some latitudes and unrealistic at others. This is a minor concern because the linear analytical solutions, which simply scale with the forcing amplitude, seem to describe important components of the nonlinear response, and because the nonlinear mechanisms explored here seem fairly insensitive to the forcing amplitude. Overall, the hierarchy of analytical and numerical results presented highlights robust aspects of the response to tropical and subtropical zonally asymmetric torques and represents the first step toward understanding the response in fully comprehensive general circulation models.

Section 2 describes the linear analytical Gill model response to a prescribed torque and contrasts it with the

response to a prescribed diabatic heating. Section 3 discusses the nonlinear response in idealized general circulation model (GCM) simulations in the absence and presence of basic-state baroclinicity. The results are summarized and discussed in section 4.

2. The Gill model response

The Gill (1980) model of the tropical atmosphere (see also Matsuno 1966) is perhaps the simplest analytical model that illustrates the basic features of the tropical large-scale circulation. When forced with zonally asymmetric diabatic heating distributions, it qualitatively represents the Walker and Hadley circulations and the various tropical wave modes. Here the well-known Gill model response to a prescribed zonally asymmetric diabatic heating will be compared and contrasted with the response to a zonally asymmetric torque. The method used to find linear solutions to a prescribed first-baroclinic torque is described in detail in the appendix and the solutions are presented in the remainder of this section. It should be remembered that the Gill model represents a first baroclinic mode and therefore a prescribed torque will project only onto this mode and thus have opposite signs at upper and lower levels, whereas a diabatic heating will be of a single sign with a midlevel maximum. In particular, the vertical derivative of a torque can be related to the horizontal derivative of a diabatic heating through thermal wind balance. Note also that the model includes dissipation in the momentum equation in the form of a Rayleigh drag.[1]

Figure 1 (top left) shows a schematic of vertical structure of the diabatic (dashed) and mechanical (solid) forcings imposed in the Gill model. We will compare the solutions for hemispherically symmetric forcings centered at the equator that project onto the zeroth-order parabolic cylinder function (called Q0 and $\mathcal{F}0$, respectively). We will also compare the response to hemispherically asymmetric forcings that are centered in the NH and project onto both the zeroth and first parabolic cylinder functions (called Q0 + Q1 and $\mathcal{F}0 + \mathcal{F}1$, respectively). The forcings are imposed with a cosine structure in longitude with unit amplitude (see Fig. 1, top right) and with an analytical structure as in (3.15) from Gill (1980). The thermal perturbation is always prescribed as a positive heating, while the mechanical forcing is always westward at upper levels. Using the same velocity and time scales as Gill (1980) of 60 m s^{-1} and 0.2 days, respectively, the dimensional magnitude of a unit $\mathcal{F}0$ forcing is 290 m s^{-1} day^{-1}. This is much larger than typical torques we expect to observe in the real atmosphere. The response to a torque of more realistic magnitude is explored in idealized GCM simulations presented in the next section. Note that in contrast with many previous studies of the Gill model we will focus on the mid- to upper-level response.

Figure 2 (top left) shows the upper-level horizontal flow and the midlevel vertical velocity response in the Gill model to a prescribed zonally asymmetric diabatic heating applied at the equator, which is outlined by the green contour. The response is identical to Figs. 1a–c in Gill (1980) except that here we show upper-level horizontal winds. There is strong upwelling in the region of the imposed heating and weak downwelling to the east and west. The horizontal structure of the response is consistent with a Kelvin wave pattern to the east and a planetary Rossby wave pattern to the west. Figure 2 shows the corresponding zonally averaged streamfunction and zonal wind responses (top right). The response is identical to Fig. 1d in Gill (1980) and has strong equatorial upwelling and a characteristic Hadley cell structure on both sides of the equator. There is eastward flow aloft and westward flow at the surface both north and south of the equator, which is consistent with advection of planetary vorticity by the zonal-mean Hadley flow. The meridional-mean response has a characteristic Walker cell structure with upwelling centered on the heating and downwelling to the east and west (not shown).

Figure 2 (bottom) shows the Gill model response to a zonally asymmetric torque applied at the equator. The vertical velocity response is not collocated with the prescribed torque, which is outlined by the green contour (bottom left). Instead there is downwelling to the west both north and south of the equator and equatorial upwelling to the east. The horizontal structure of the response to the west is consistent with a Rossby wave pattern similar to the Q0 forcing. To the east the response is consistent with a Kelvin wave pattern but it has the opposite sign to that of Q0 and thus produces westward flow and upwelling to the east of the torque. There is upper-level westward flow along the equator in the zonal mean (Fig. 2, bottom right). The zonally averaged meridional streamfunction response is identical to that for Q0 (cf. Fig. 2, right). This must be the case if both forcings are of unit amplitude with a zeroth parabolic cylinder function structure in the meridional direction, which can be seen after the momentum, continuity, and thermodynamic equations are combined into a single equation and the zonal mean is taken; for instance,

[1] Rayleigh drag is used in the linear Gill model to obtain a steady-state circulation. In the nonlinear context the circulation can be maintained by angular momentum conservation (Held and Hou 1980). Free-tropospheric Rayleigh drag is typically not prescribed in GCMs.

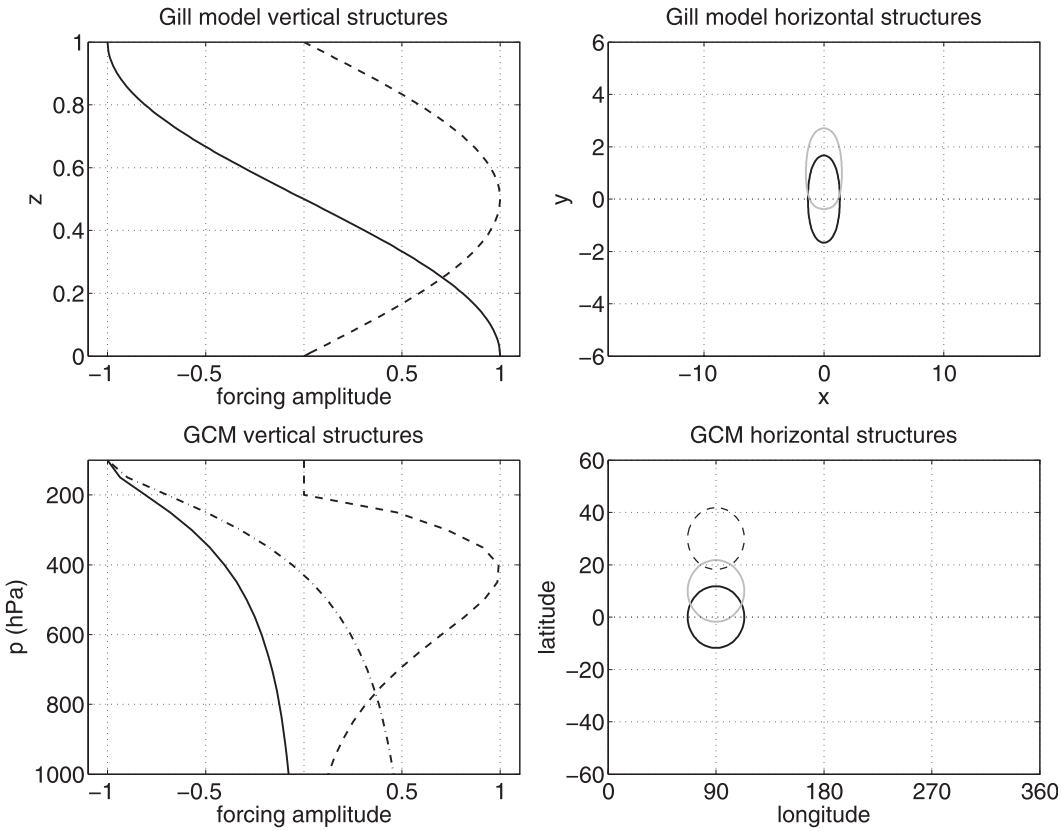

FIG. 1. (left) Vertical structure of the prescribed diabatic heating (dashed) and first baroclinic mode torque (solid) in (top) the analytical Gill (1980) model and (bottom) the idealized GCM simulations. A predominantly upper-level torque (dashed–dotted) was also imposed in the GCM. (right) Horizontal structure of (top) the prescribed equatorially symmetric (black) and asymmetric (gray) cosine forcings imposed in the Gill (1980) model and (bottom) the prescribed 0° (black), 10° (gray), and 30°N (dashed) Gaussian torques imposed in the GCM simulations. All forcings are normalized to have a peak amplitude with a nondimensional magnitude of unity.

$$\epsilon^2\overline{v} + \frac{1}{4}y^2\overline{v} - \frac{\partial^2\overline{v}}{\partial y^2} = \begin{cases} \dfrac{\partial\overline{Q}}{\partial y} & \text{for the diabatic heating,} \\ -\dfrac{1}{2}y\overline{\mathcal{F}} & \text{for the torque,} \end{cases} \tag{1}$$

where an overbar denotes a zonal average [see (2.10) from Gill (1980) for the diabatic heating and (A1) for the torque]. Note that the equivalence of the zonal-mean streamfunction responses to Q0 and $\mathcal{F}0$ cannot be used to infer the relative strength of responses because Q0 in the Gill (1980) model is proportional to the thermal forcing with the constant of proportionality dependent on the assumed relationship between moist convective heating and horizontal mass convergence (e.g., Zebiak 1982; Neelin 1989; Neelin and Held 1987). We make no assumptions here about the value of this proportionality constant.

Overall, there are both similarities and striking differences in the Gill model response to an equatorial zonally asymmetric diabatic heating and torque. A mid-tropospheric equatorial heating and an upper-level equatorial westward torque both produce a zonal-mean meridional circulation with upwelling on the equator and subsidence in the subtropics. They also have upper-level anticyclonic Rossby wave gyres centered to the northwest and southwest of the forcing leading to westward flow to the west of the forcing. However, to the east of the forcing the zonal wind responses differ. The upper-level flow is eastward in response to the heating with the ascending phase of the Kelvin wave in phase with the diabatic heating and provides the adiabatic cooling needed to balance the heating. In contrast, upper-level flow is westward in response to the torque with the ascending phase of the Kelvin wave to the east of the torque. The vertical motion must be balanced by Newtonian cooling and thus is comparatively weaker in amplitude and broader in spatial extent.

When the diabatic heating is prescribed as a linear combination of the first two parabolic cylinder functions

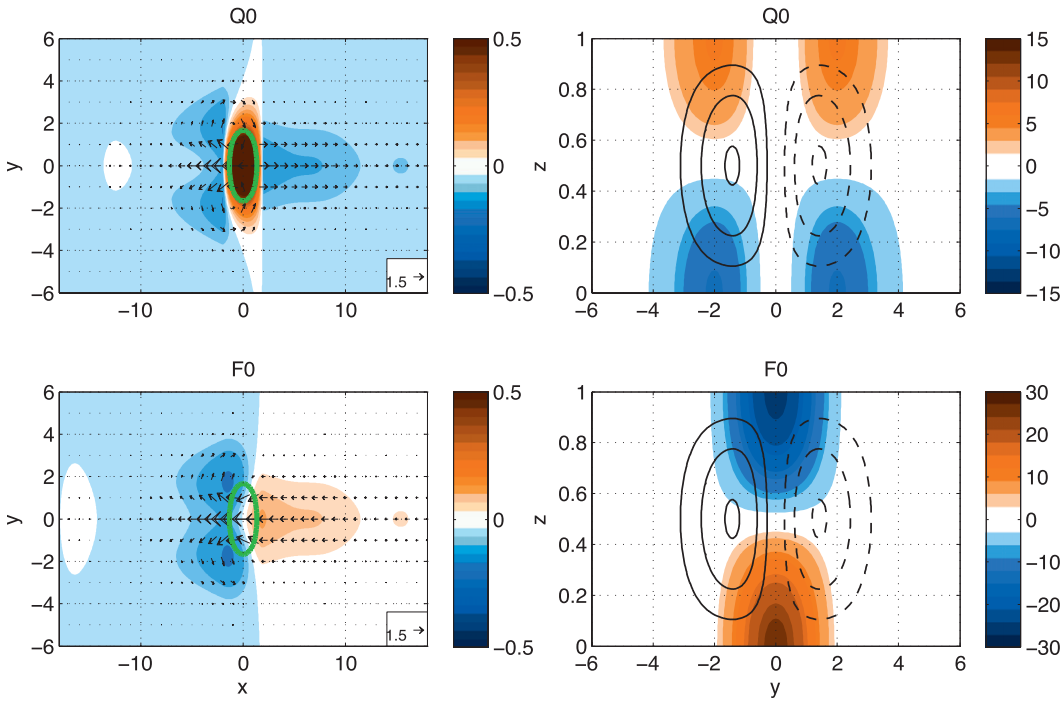

FIG. 2. The Gill (1980) model response to the (top) Q0 heating and (bottom) $\mathcal{F}0$ torque. (left) Upper-level horizontal flow (arrows) and midlevel vertical velocity (shading) responses. (right) Zonal-mean streamfunction (contours, dashed clockwise) and zonal-mean zonal wind (shading) responses. The green contour is the 0.5 forcing isoline.

(Q0 + Q1) it is displaced into the NH subtropics, which produces an idealization of the observed Southern Hemisphere (SH) winter diabatic heating distribution. Figure 3 (top) shows the Gill model response to such a diabatic heating, which is outlined by the green contour. Once again, the response is identical to Fig. 3 in Gill (1980) except that upper-level horizontal winds are shown here. The horizontal flow and vertical velocity responses (upper left) are qualitatively similar to that for the equatorial diabatic heating except that the response is stronger and no longer meridionally antisymmetric about the diabatic heating. The Rossby wave gyres are still present and the upwelling is still centered over the diabatic heating, but there is now strong downwelling both west of the diabatic heating and in the SH subtropics. The zonal-mean upwelling is displaced into the NH and there is a strong cross-equatorial Hadley flow and a weak summer cell in the NH subtropics.

When the zonally asymmetric torque is displaced into the NH subtropics the upper-level horizontal response is once again qualitatively similar to the equatorial torque response but with a breaking of meridional symmetry (Fig. 3, bottom). The main differences are the enhanced downwelling to the northwest of the torque, weaker downwelling to the southwest, and the displacement of the Rossby wave gyres into the NH (bottom left). The zonal-mean response is dramatically different from the response to Q0 + Q1; the zonal-mean upwelling is displaced into the SH with a strong cross-equatorial Hadley flow. The main overturning cell is about twice as wide meridionally as that produced by the off-equatorial diabatic heating. The existence of poleward flow in the region of the westward forcing, with the overturning cell centered below the forcing, is reminiscent of the downward control circulation response to a prescribed torque (Haynes et al. 1991). However, the downward control theory is inviscid outside of the boundary layer and in the steady-state limit produces a mean meridional circulation response strictly below the torque (Holton et al. 1995). Note that the Gill (1980) model includes free-tropospheric Rayleigh drag and therefore the circulation response can extend beyond the prescribed torque.

The differences in horizontal flow and vertical velocity responses to zonally asymmetric off-equatorial diabatic heatings and torques are similar to those for the equatorial forcings. However, there are striking differences in the zonal-mean streamfunction responses. In response to the heating the zonal-mean upwelling occurs in the NH while in response to the torque it occurs in the SH. The upwelling response to the heating is determined directly by the position of the heating according to a weak-temperature gradient balance (Sobel and Bretherton 2000;

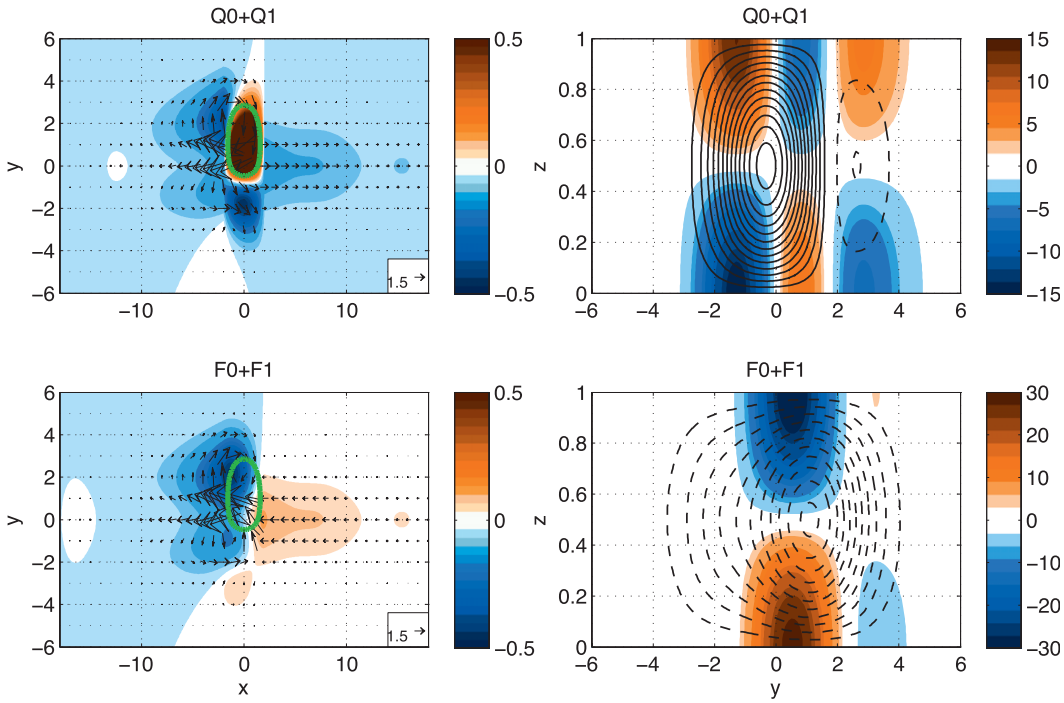

FIG. 3. As in Fig. 2, but for (top) the Q0 + Q1 heating and (bottom) the $\mathcal{F}0 + \mathcal{F}1$ torque.

Sobel et al. 2001). In contrast, the zonal-mean upwelling response to the torque is inferred from the zonal-mean meridional velocity response similar to a downward control–type balance (Haynes et al. 1991). These different balances are explored further in the next section.

3. Response in an idealized general circulation model

a. Model description

The Gill (1980) model discussed in section 2 is based on linear dynamics and hence represents the linear response to a prescribed zonally asymmetric force. The nonlinear response can be studied numerically using a dry primitive equation model of the atmosphere with simplified physics. Here we use the National Center for Atmospheric Research's (NCAR's) Community Atmosphere Model, version 5 (CAM 5.0; Neale et al. 2010) with idealized physics (Rayleigh drag and Newtonian temperature relaxation) and a resolution of 1.9° × 2.5° × 30 vertical levels[2] to study the nonlinear response to a prescribed zonally asymmetric torque.

Two model configurations are used. The first configuration (discussed in section 3b) is qualitatively consistent with the linear Gill (1980) model. There is Rayleigh drag and Newtonian cooling throughout the domain with time scales of 30 and 10 days, respectively. The model uses an η vertical coordinate that, since there is no topography and a model top near 0 hPa, reduces to $\eta \sim p/p_s$, where p_s is surface pressure. The reference temperature profile for $\eta > 0.1$ is

$$\theta_{\mathrm{ref}} = \theta_0 - \Delta\theta \ln(\eta), \tag{2}$$

where θ is potential temperature, θ_0 is 299 K, and $\Delta\theta$ is 35 K. For $\eta < 0.1$, the temperature T is prescribed to increase by 40 K from $\eta = 0.1$ to $\eta = 0$. This temperature profile provides a reasonable fit to the time- and tropical-mean sounding from the 40-yr European Centre for Medium-Range Weather Forecasts (ECMWF) Re-Analysis (ERA-40), which has slightly enhanced static stability in the upper troposphere and strongly enhanced stability in the stratosphere. This model configuration is similar to that used by Norton (2006, hereafter N06).

The second model configuration (discussed in section 3c) is identical to the Held and Suarez (1994, hereafter HS94) configuration. The HS94 configuration is substantially different from the N06 configuration. It has different radiative equilibrium temperature and momentum damping profiles. The radiative equilibrium temperature profile increases by about 10 K in potential temperature

[2] Simulations denoted by "hres" were run at 0.9° × 1.25° × 30 vertical levels.

TABLE 1. Summary of nonlinear model simulations with Gaussian forcings. The location refers to the location of the peak forcing, structure refers to the vertical structure of the torque [baroclinic (BC) or single signed (SS)], and MTG refers to whether there is a meridional temperature gradient [yes (Y) or no (N)].

Simulation name	Configuration	Forcing	Location	Structure	MTG
norQ0	N06	Heating	0°N	—	N
norF0hres	N06	Torque	0°N	BC	N
norQ0 + Q1	N06	Heating	10°N	—	N
norF0 + F1	N06	Torque	10°N	BC	N
norF0Nhres	N06	Torque	0°N	SS	N
norF10N	N06	Torque	10°N	SS	N
norF30N	N06	Torque	30°N	SS	N
HSdef0N	HS94	Torque	0°N	SS	Y
HSdef10N	HS94	Torque	10°N	SS	Y
HSdef30N	HS94	Torque	30°N	SS	Y
HSef0N	HS94	Torque	0°N	SS	N

through the depth of the troposphere and is isothermal in the stratosphere. The Rayleigh drag time scale varies from 1 day near the surface to infinity above the $\eta = 0.7$ level, and the Newtonian cooling time scale varies from 4 days near the surface to 40 days in the free troposphere. The HS94 configuration is used to examine the influence of baroclinic eddies in the basic state on the response to the imposed torques. Because it would not be obvious whether differences between our two model configurations would be due to the existence of baroclinic eddies in the basic state or differences in damping and radiative equilibrium temperature profiles, we perform an additional run with the HS94 configuration but without a meridional gradient in the radiative equilibrium temperature.

The forcings prescribed in the idealized GCM simulations are Gaussian in longitude and latitude. While this differs from the sinusoidal structure in longitude used in the Gill (1980) model, it is consistent with previous studies (Haynes et al. 1991; Shepherd et al. 1996; N06; Ring and Plumb 2007; Chen and Zurita-Gotor 2008). In all of the model simulations described below the torque is centered at 90°E with a standard deviation (i.e., a horizontal scale) of 20°. The sensitivity of the response to the position of the Gaussian torque is explored by centering the torque at 0°, 10°, and 30°N (see Fig. 1, bottom right). In all cases the meridional standard deviation (length scale) is 10°. The different latitudinal locations of the torque are meant to mimic the varied locations of torques associated with parameterized OGWD and CMT [see Fig. 11 in McFarlane (1987) and Fig. 1 in Richter and Rasch (2008)]. The diabatic heating is also prescribed as a Gaussian in latitude with the same structure as the torque and a Gaussian in height centered at 420 hPa for consistency with N06. Since the model effectively uses a hybrid σ-pressure coordinate, the heating is prescribed in log-pressure z^* coordinates for pressures larger than 200 hPa as

$$Q(p) = Q_0 \exp\left\{-\frac{\left[\ln\left(\frac{420\,\mathrm{hPa}}{p_s}\right) - \ln\left(\frac{p}{p_s}\right)\right]^2}{2\Delta\eta^2}\right\}, \tag{3}$$

where $\Delta\eta = 0.42$ specifies the vertical scale of the diabatic heating and $p_s = 1000$ hPa is the nominal surface pressure. A peak diabatic heating rate of $Q_0 = 5$ K day^{-1} is prescribed, and Q is set to zero above 200 hPa (see Fig. 1, bottom left, dashed line).

For the mechanical forcing, we treat the tropopause as the equivalent to the model top of the Gill (1980) model and choose a lognormal vertical distribution for the forcing from the surface up to 100 hPa; that is,

$$\mathcal{F}(p) = \begin{cases} \mathcal{F}_0 \dfrac{p_s}{p} \exp\left\{-\dfrac{1}{2}[\ln(p) - B]^2\right\} - \mathcal{F}_{\mathrm{bt}} & \text{for purely baroclinic torques,} \\ \mathcal{F}_0 \dfrac{p_s}{p} \exp\left\{-\dfrac{1}{2}[\ln(p) - B]^2\right\} & \text{for single-signed torques,} \end{cases} \tag{4a}$$

$$\mathcal{F}_{\mathrm{bt}} = \frac{1}{p_s - 100\,\mathrm{hPa}} \int_{p_s}^{100\,\mathrm{hPa}} \mathcal{F}_0 \frac{p_s}{p} \exp\left\{-\frac{1}{2}[\ln(p) - B]^2\right\} dp, \tag{4b}$$

where $B = 10.25$ and $\mathcal{F}_0 = -3.3$ m s^{-1} day^{-1}. Above 100 hPa, $\mathcal{F}$ is set to zero. The constant $\mathcal{F}_{\mathrm{bt}}$ is a barotropic forcing defined simply as the vertical mean of the first term on the right-hand side of (4a) and is subtracted from some torques in order to give them opposite signs at upper and lower levels (see Fig. 1, bottom left, solid and dashed–dotted lines). According to these parameters the baroclinic torque has an extremum of -13 m s^{-1} day^{-1} at 90°E and -1.8 m s^{-1} day^{-1} in the zonal mean, while the single-signed torque has an extremum of -19 m s^{-1} day^{-1} at 90°E and -2.5 m s^{-1} day^{-1} in the zonal mean. The single-signed torque is westward at

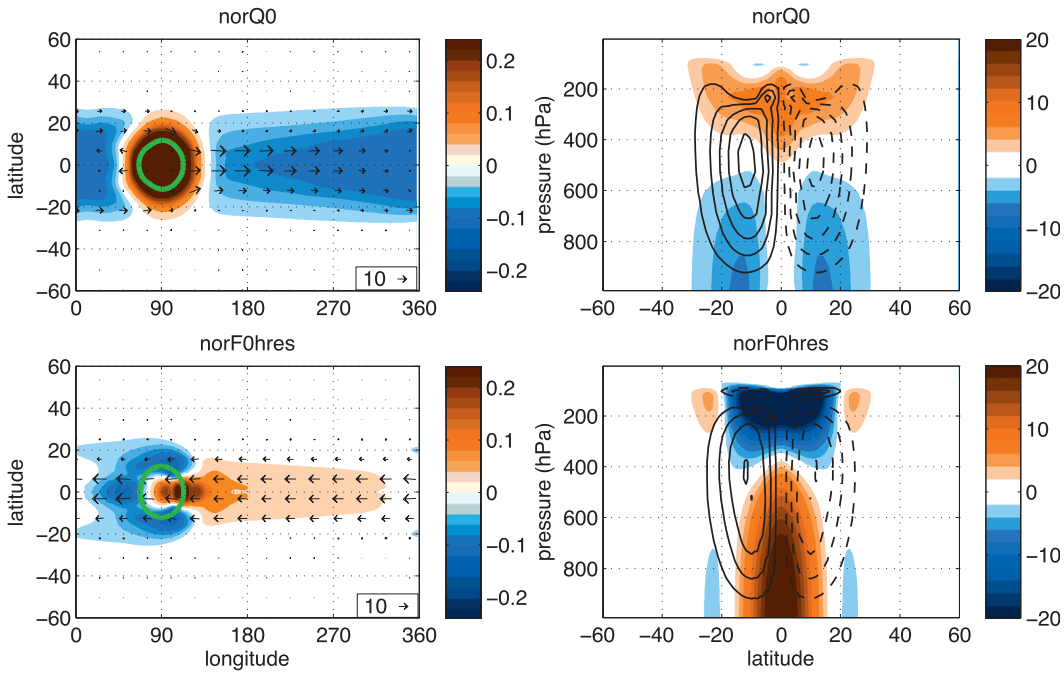

FIG. 4. The nonlinear GCM response to the (top) Q0 heating and (bottom) $\mathcal{F}0$ torque in the N06 configuration. (left) Horizontal flow at 273 hPa (arrows) and 525-hPa vertical velocity (shading, contour interval (CI) = 0.02 cm s^{-1}, positive upward) responses. (right) Zonal-mean streamfunction (contours, dashed clockwise, CI = 2×10^9 kg s^{-1}) and zonal-mean zonal wind (shading, CI = 2 m s^{-1}) responses. The green contour marks the location where the forcing has half of its peak amplitude.

all heights to make it a better analog for OGWD, which is typically strongly westward in the upper troposphere/lower stratosphere and decays toward zero near the earth's surface (e.g., Lilly and Kennedy 1973; Palmer et al. 1986; McFarlane 1987). (Note, however, that the vertical structure of the idealized torque does not properly capture the structure of OGWD.) For comparison, OGWD in CAM using realistic boundary conditions peaks near -50 m s^{-1} day^{-1} over the Tibetan plateau during January (not shown). In all cases the model is run for 10 yr with the first 200 days of integration regarded as "spinup" time and therefore discarded. A summary of the model experiments and the applied forcings can be found in Table 1.

b. *Response in the absence of midlatitude baroclinic eddies*

Figure 4 (left) shows the nonlinear upper-level horizontal flow response at 273 hPa and vertical velocity response at 520 hPa to the equivalent Q0 diabatic heating (top) and $\mathcal{F}0$ baroclinic Gaussian torque (bottom) both centered at the equator and 90°E and outlined by the green contour. The model configuration is similar to N06; it includes a prescribed Rayleigh drag damping throughout the atmosphere. There are qualitative similarities between the linear and nonlinear responses, such as ascent to the east of the torque, subsidence with off-equatorial maxima to the west of the torque, and a similar phasing of equatorial westward and eastward flow relative to the forcings [cf. Figs. 4 and 2 (left panels)]. However, substantial differences also exist. In particular, the nonlinear response to both forcings exhibits subsidence that is more meridionally confined, weaker horizontal winds to the west of the heating, and more zonally symmetric zonal winds. The enhanced zonally symmetric component of the response to the heating was also seen in N06 (see their Fig. 6c) and could be due to a number of factors: nonlinear momentum advection, EP fluxes, the different structure of the forcing (Gaussian versus cosine), or the fact that the domain is periodic in the nonlinear simulation.[3] Figure 4 (right) shows the corresponding zonal-mean streamfunction and zonal wind responses to the diabatic heating (top) and torque (bottom). For both forcings the zonal-mean streamfunction responses are qualitatively similar to the linear analytical model response. There are shallow circulation cells of opposite sign above the main Hadley cells in response to the torque, which are the result of the change in

[3] When a region of strong damping is imposed east of the torque (near 300°E), the zonally symmetric component of the response is weakened suggesting that the periodicity of the domain does impact the response to the torque.

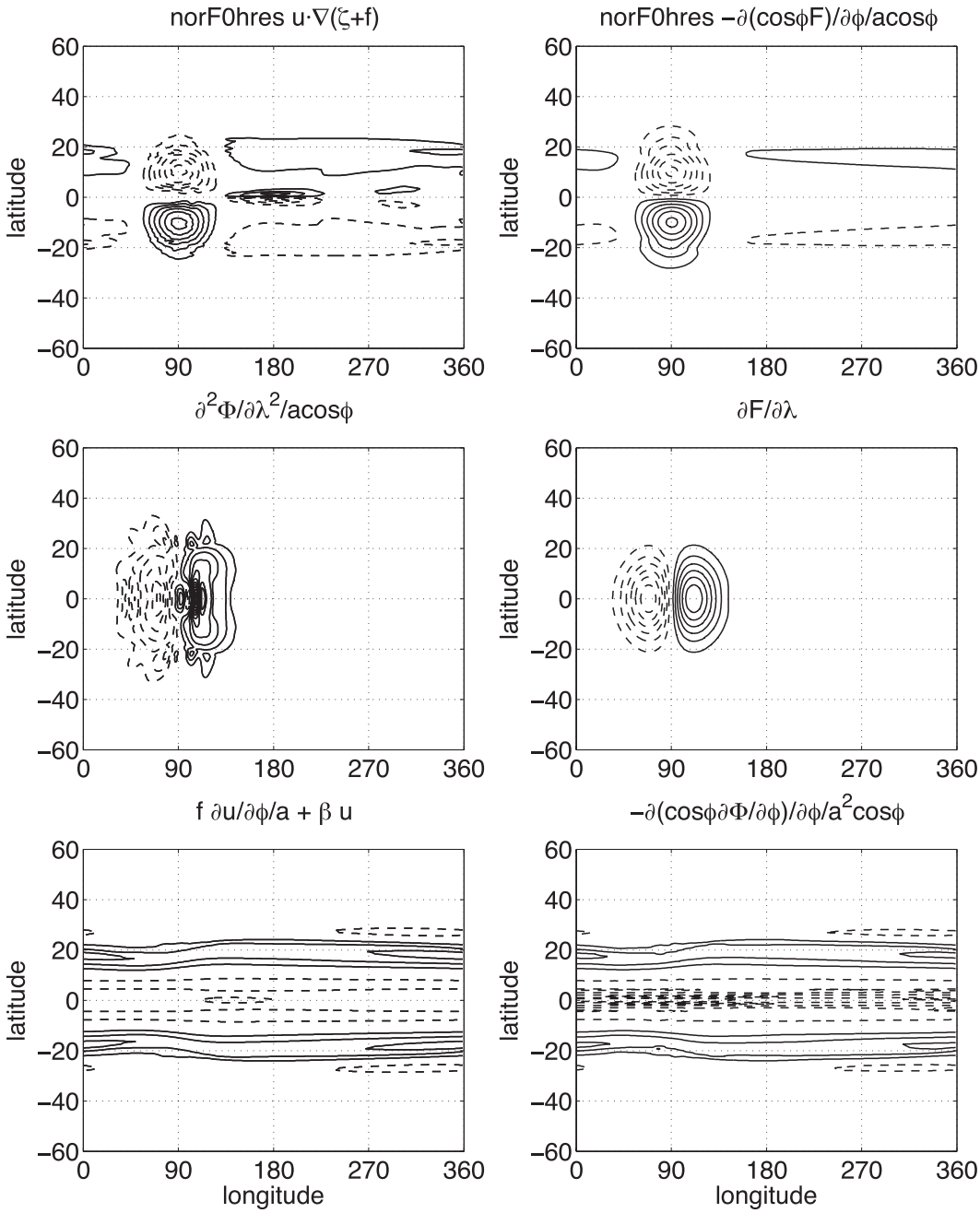

FIG. 5. The nonlinear GCM vorticity and divergence budget responses to the $\mathcal{F}0$ torque at 142 hPa for the N06 configuration. (top) (left) Horizontal vorticity advection and (right) meridional gradient of the torque contributions to the vorticity budget. CI is 1×10^{-11} s^{-1}. (middle) Contributions of the zonal momentum balance to the divergence budget. CI is 0.25×10^{-11} s^{-1}. (bottom) Contributions of the meridional momentum balance to the divergence budget. CI is 2×10^{-10} s^{-1}.

sign of the vertical derivative of the torque. In the analytical model this change in sign is not present (cf. solid lines in left panels of Fig. 1). In general the zonal-mean zonal wind responses are also in agreement with the exception of the upper-level equatorial eastward flow in the nonlinear response to Q0, which was noted previously by N06.

The nonlinear upper-level response to the torque can be further understood using the vorticity and divergence budgets. Figure 5 (top) shows the dominant terms in the vorticity budget at 142 hPa in the vicinity of the torque, namely the horizontal advection of absolute vorticity and the meridional gradient of the torque—that is,

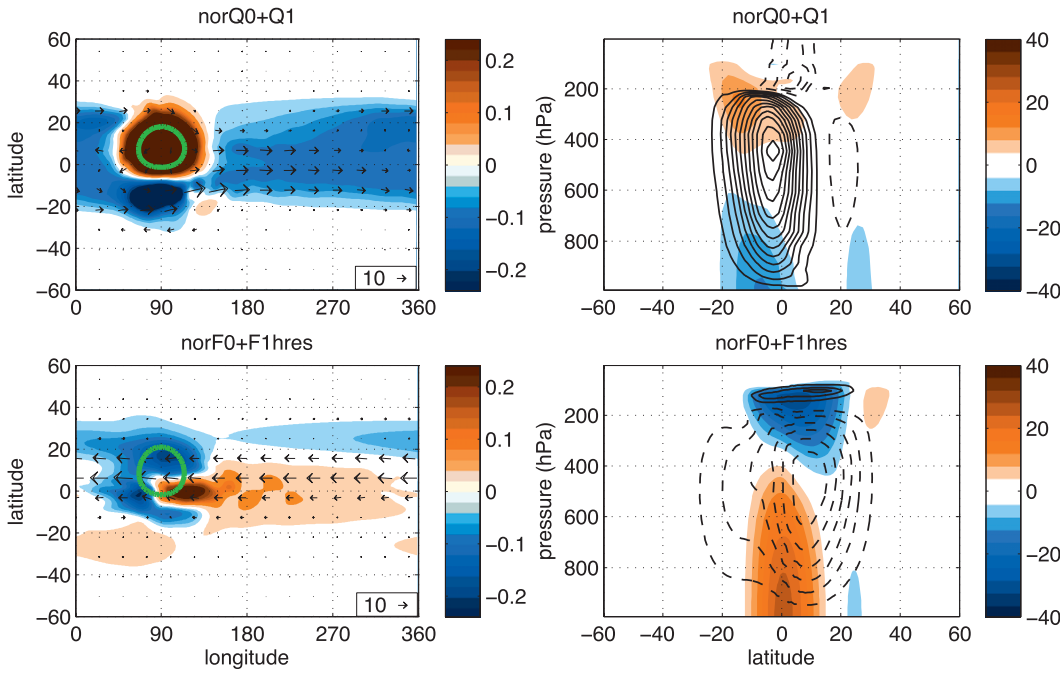

FIG. 6. As in Fig. 4, but for the (top) Q0 + Q1 heating and (bottom) $\mathcal{F}0 + \mathcal{F}1$ torque. CI is 4×10^9 kg s^{-1} for the streamfunction and 4 m s^{-1} for zonal-mean zonal wind.

$$\mathbf{u} \cdot \nabla(\zeta + f) \approx -\frac{1}{a\cos\phi}\frac{\partial}{\partial\phi}(\cos\phi\mathcal{F}), \tag{5}$$

where $\mathbf{u}$ is the horizontal velocity, ζ is the vertical component of the vorticity, f is the Coriolis parameter, ϕ is latitude, and $\mathcal{F}$ includes both the applied torque and the Rayleigh drag. Note that the full vorticity budget is given in (7) of Sardeshmukh and Held (1984). The left-hand side is dominated by planetary vorticity advection, indicating a nearly linear balance that can be used to infer the meridional wind response. Recall that in response to an imposed diabatic heating the advection of planetary vorticity by the equatorward flow balances negative vortex stretching in the region of horizontal divergence [see (4.11) in Gill (1980) and Fig. 10 in N06]. In contrast to the response to the heating, the divergent wind response to the torque is not constrained by the balance between diabatic heating and adiabatic cooling; thus, we appeal to the divergence balance to understand the divergent wind response. Figure 5 shows the dominant terms in the divergence budget at 142 hPa (middle and bottom). The divergence balance can be divided into two balances, for instance,

$$\frac{f}{a}\frac{\partial u}{\partial\phi} + \beta u \approx -\frac{1}{a^2\cos\phi}\frac{\partial}{\partial\phi}\left(\cos\phi\frac{\partial\Phi}{\partial\phi}\right), \tag{6a}$$

$$\frac{1}{a\cos\phi}\frac{\partial^2\Phi}{\partial\lambda^2} \approx \frac{\partial\mathcal{F}}{\partial\lambda}, \tag{6b}$$

which produce zonally symmetric and zonally asymmetric responses, respectively. Note that the full divergence budget is given in (19) of Stevens (1979). These balances reflect those from the meridional momentum (geostrophic balance) and zonal momentum equations, respectively. Note that the vorticity [(5)] and divergence [(6)] balances can be combined to obtain the divergent wind response to the equatorial torque; that is,

$$\delta = \frac{1}{a\cos\phi}\frac{\partial u}{\partial\lambda} + \frac{1}{a\cos\phi}\frac{\partial}{\partial\phi}(\cos\phi v) \approx -\frac{1}{fa\cos\phi}\frac{\partial}{\partial\phi}(\cos\phi\mathcal{F}) - \frac{1}{a^2\cos\phi}\frac{\partial}{\partial\phi}\left[\frac{1}{\beta}\frac{\partial}{\partial\phi}(\cos\phi\mathcal{F})\right]. \tag{7}$$

The full linear solution could be obtained in combination with the continuity and enthalpy equations along with hydrostatic balance and would be similar to inferring the balanced weak-temperature gradient response to a diabatic heating (Sobel et al. 2001). We will explore this in more detail in a future study.

Figure 6 (left) shows the corresponding horizontal flow response at 273 hPa and vertical velocity response

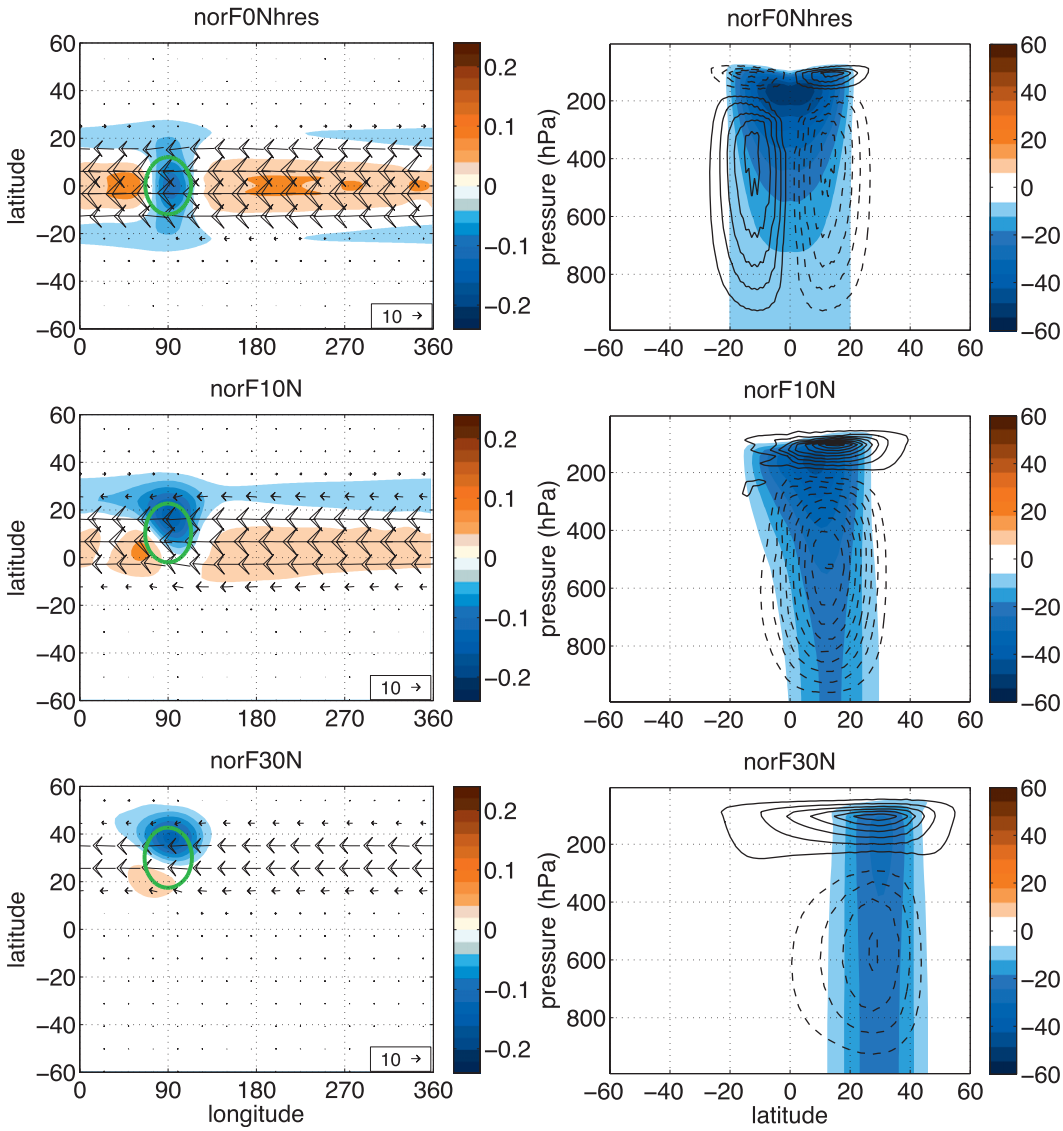

FIG. 7. As in Fig. 4, for single-signed torques centered at (top) 0°, (middle) 10°, and (bottom) 30°N. CI is 0.02 cm s^{-1} for vertical velocity, 2×10^9 kg s^{-1} for the streamfunction, and 4 m s^{-1} for the zonal-mean zonal wind.

at 520 hPa to the equivalent Q0 + Q1 diabatic heating (top) and $\mathcal{F}0 + \mathcal{F}1$ baroclinic Gaussian torque (bottom). Again, the vertical velocity responses are qualitatively similar to the analytical Gill model responses though the horizontal wind responses are more zonally symmetric (cf. left panels of Figs. 6 and 3). The responses involve the strengthening and displacement of the equatorial forcing responses into the NH. Figure 6 (right) shows the corresponding zonal-mean streamfunction and zonal wind responses to the diabatic heating (top) and torque (bottom). Once again both responses are in good agreement with the respective linear analytical responses; zonal-mean upwelling occurs in the NH (SH) in response to the heating (torque). For the case of the torque, the circulation cell is in close alignment with the torque as might be expected from downward-control theory (Haynes et al. 1991). As for the equatorial torque, there is an additional shallow circulation cell of opposite sign above the cross-equatorial circulation that cannot be represented in the analytical model.

As discussed in the introduction, vertical momentum transfers associated with CMT and OGWD occur throughout the subtropics and therefore it is relevant to consider the response to a prescribed torque that is localized off the equator. Figure 7 shows the nonlinear horizontal flow response at 273 hPa and vertical velocity response at 520 hPa (left) and the zonal-mean streamfunction and zonal wind (right) responses to a prescribed

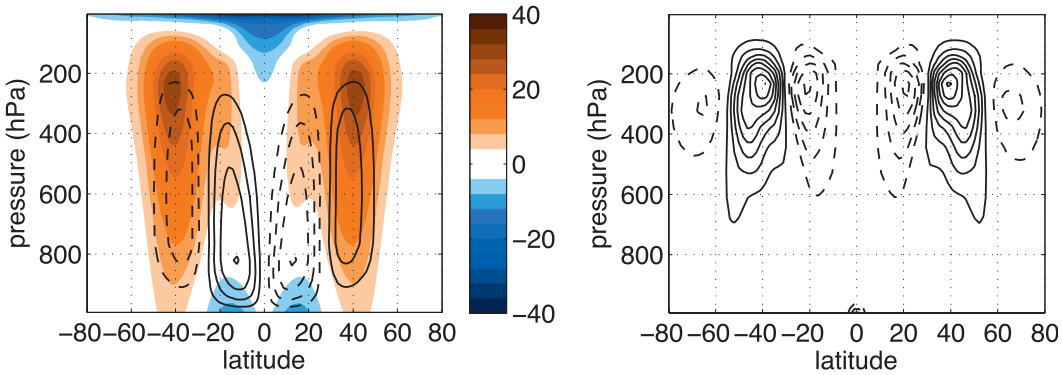

FIG. 8. HS94 zonal-mean basic state. (left) Zonal-mean zonal wind (shading) and streamfunction (contours). (right) Horizontal eddy momentum flux convergence; that is, $-(1/a\cos^2\phi)\partial(a\cos^2\phi\overline{u'v'})/\partial\phi$, where the overbar represents a time and zonal average and the prime is a deviation from the zonal average. CI is 2×10^{10} kg s^{-1} for the streamfunction, 4 m s^{-1} for zonal-mean zonal wind, and 0.5 m s^{-1} day^{-1} for the horizontal eddy momentum flux convergence (with dashed contours denoting negative values).

zonally asymmetric torque at (top) 0°, (middle) 10°, and (bottom) 30°N. The torques in this case are single-signed torques according to (4a) and thus project strongly onto barotropic and baroclinic vertical modes. The response to the single-signed equatorial torque shows a somewhat different horizontal structure compared to the baroclinic torque [cf. Fig. 4 (bottom left) and Fig. 7 (top left)]. Downwelling in the vicinity of the torque is much stronger for the single-signed torque, suggesting that the barotropic component of the torque induces local subsidence. However, the zonal-mean streamfunction responses are in good agreement [cf. Fig. 4 (bottom right) and Fig. 7 (top right)].

When the torque is placed at 10°N, the response involves strong downwelling to the northeast and upwelling to the southwest and is somewhat similar to the $\mathcal{F}0+\mathcal{F}1$ response in the nonlinear and linear analytical models but with a slight clockwise rotation of the response about the center of the forcing. It also has a strong zonally symmetric component, as noted previously. The zonal-mean streamfunction response involves upwelling in the SH and downwelling in the NH, which is also similar to the $\mathcal{F}0+\mathcal{F}1$ response. The zonal-mean zonal wind response is westward all the way to the surface, consistent with a torque that is westward at all levels. Finally, when the torque is placed at 30°N, the vertical velocity response becomes zonally confined with downwelling to the northeast and upwelling to the southwest of the torque. The vorticity balance to the south of the torque (not shown) is identical to (5); however, to the north it is

$$f\delta + \mathbf{u}\cdot\nabla(\zeta+f) \approx -\frac{1}{a\cos\phi}\frac{\partial}{\partial\phi}(\cos\phi\mathcal{F}). \qquad (8)$$

Note that in the zonal mean the balance in (8) is similar to the meridional derivative of the downward-control balance (Haynes et al. 1991). The meridional momentum contribution to the divergence balance in response to the subtropical torque (not shown) is similar to (6a); however, the zonal momentum contribution becomes

$$-f\frac{\partial v}{\partial\lambda} + \frac{1}{a\cos\phi}\frac{\partial^2\Phi}{\partial\lambda^2} \approx \frac{\partial\mathcal{F}}{\partial\lambda}. \qquad (9)$$

Clearly the balances in (8) and (9) only hold sufficiently far from the equator where f is not very close to zero. Once again the zonal-mean streamfunction response involves a clockwise circulation and the zonal wind response is westward with a significant barotropic component.

c. *Response in the presence of midlatitude baroclinic eddies*

Here we investigate how the responses to the prescribed zonally asymmetric torques discussed in the previous section are modified in the presence of midlatitude baroclinicity in the basic state. The nonlinear simulations are repeated in a HS94 configuration, which prescribes a large-scale meridional temperature gradient in the radiative equilibrium temperature (see page 1826 of HS94). Figure 8 shows the time- and zonal-mean basic state streamfunction and zonal wind (left) and horizontal eddy momentum flux convergence (HEMFC; right) in the HS94 configuration [i.e., $-(1/a\cos^2\phi)\partial(a\cos^2\phi\overline{u'v'})/\partial\phi$, where the overbar represents a time and zonal average, the prime is a deviation from the zonal average, and a is the radius of the earth]. The upper-level eastward flow in midlatitudes coincides with regions of large HEMFC and the indirect Ferrel cells.

Figure 9 shows the anomalous horizontal flow response at 273 hPa and vertical velocity response at 520 hPa (left) and the zonal-mean streamfunction and zonal wind (right) responses when a zonally asymmetric torque is placed at

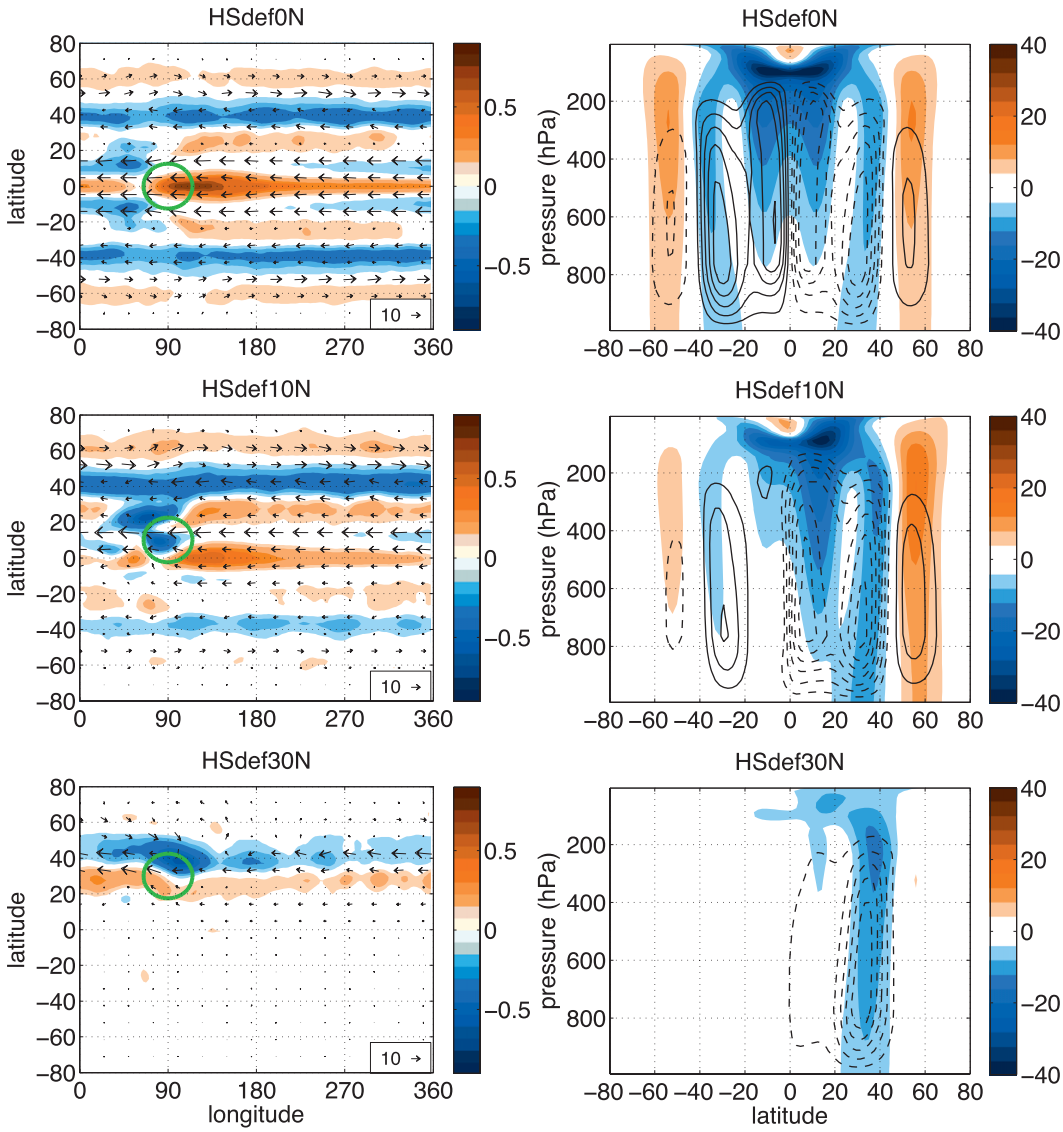

FIG. 9. As in Fig. 4, but for single-signed torques in the HS94 configuration centered at (top) 0°, (middle) 10°, and (bottom) 30°N. All quantities are anomalies relative to the basic state shown in Fig. 8. CI is 0.07 cm s^{-1} for vertical velocity, 1×10^{10} kg s^{-1} for the streamfunction, and 4 m s^{-1} for the zonal-mean zonal wind.

(top) 0°, (middle) 10°, and (bottom) 30°N in the presence of midlatitude baroclinicity. All of these torques are single-signed (westward) in the vertical. The equatorial torque response between 20°S and 20°N is qualitatively similar to that in the absence of midlatitude baroclinic eddies (cf. left panels of Figs. 9 and 7). However, in the presence of baroclinicity there is no strong descent centered on the torque and the equatorial upwelling is stronger. Just poleward of 20° the downwelling–upwelling pattern in the zonal direction is reminiscent of a Walker-cell type circulation. Poleward of 30° the vertical velocity response is zonally symmetric with downwelling at 40° and upwelling at 60°. The anomalous zonal-mean streamfunction response involves strong upwelling centered on the equator and characteristic Hadley cell circulations on both sides of the equator, which is in agreement with the nonlinear response in the absence of midlatitude baroclinicity and the linear analytical response. In addition, there is an anomalous clockwise circulation between 20° and 40° and a Ferrel-type circulation between 40° and 60°, which were not seen in the absence of basic-state baroclinicity. The anomalous zonal-mean zonal wind response involves westward flow at the equator between 10°N and 10°S and extending down to 600 hPa. The zonal wind response in midlatitudes displays a barotropic structure indicating

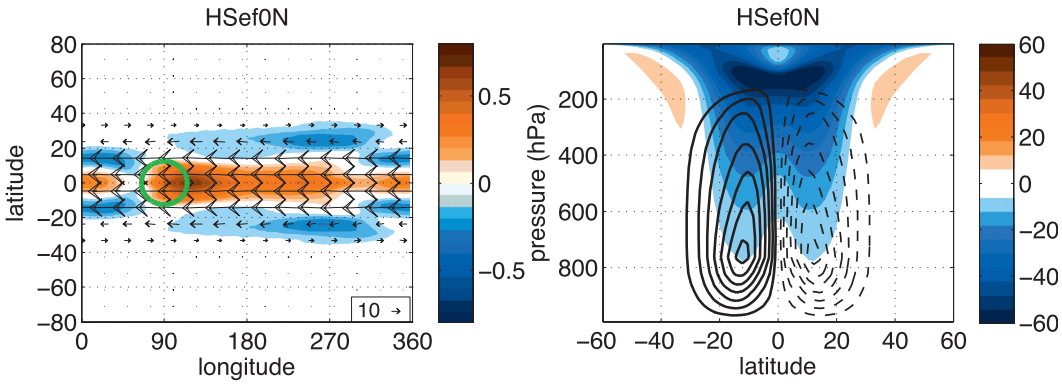

FIG. 10. As in Fig. 9, but for the response to the single-signed torque at 0° in the absence of a basic-state meridional temperature gradient in the HS94 configuration.

a poleward jet shift with a structure that is reminiscent of the northern annular mode (e.g., Thompson and Wallace 2000). Recall that in the absence of midlatitude baroclinic eddies the zonal wind response to the equatorial torque was very small poleward of 20°.

As the torque is moved to 10°N, the NH response strengthens and the SH response weakens (Fig. 9, middle left). The Walker-cell type circulation and the zonal-mean downwelling–upwelling pattern to the north of 30° are both significantly stronger. The NH zonal-mean streamfunction response strengthens and the SH response weakens (Fig. 9, middle right). There is also a larger poleward jet shift. Recall that in the absence of basic-state baroclinicity the westward zonal wind response was centered at 10°N and mostly confined to the tropics. Finally, when the torque is moved to 30°N the anomalous horizontal flow response at 273 hPa and vertical velocity response at 520 hPa are confined between 20° and 50°N (Fig. 9, bottom left). There is anomalous downwelling to the northeast and upwelling to the southwest of the torque similar to that in the absence of baroclinic eddies. The zonally symmetric upwelling and downwelling responses poleward of 40°N are stronger. In the zonal mean, the anomalous clockwise circulation and westward zonal wind responses are mostly confined between 20° and 40°N (Fig. 9, bottom right) and are reminiscent of the responses in the absence of basic-state baroclinicity (see Fig. 7).

Basic-state baroclinicity seems to have a large impact on the extratropical response to an equatorial torque. However, there are more differences between the model configurations used by N06 and HS94 than the presence of midlatitude baroclinicity in the basic state (e.g., our N06 configuration employs Rayleigh drag throughout the troposphere). The impact of baroclinic eddies can be better assessed by comparing the responses with and without a basic-state meridional temperature gradient. Figure 10 shows the horizontal flow response at 273 hPa and vertical velocity response at 520 hPa (left) and the zonal-mean streamfunction and zonal wind responses (right) to an equatorial torque in the HS94 configuration but with the radiative equilibrium temperature at all latitudes set equal to the equatorial value. The horizontal flow and vertical velocity responses between 20°N and 20°S are qualitatively similar to the responses in the presence of baroclinicity (Fig. 9). However, the vertical velocity response is qualitatively different from the response in the N06 configuration (Fig. 7, top), which is likely due to differences in the basic state and Newtonian cooling time scales (40 days in HS94 vs 10 days in N06). The response poleward of 20° is weak and does not include a Walker cell–type response or a significant zonally symmetric structure, which suggests that interactions with midlatitude baroclinic eddies produces the response poleward of 20° in Fig. 9.

The differences between the nonlinear responses in the absence and presence of baroclinicity can be further assessed using the vorticity budget. Figure 11 shows the dominant terms in the vorticity budget at 142 hPa in the vicinity of the torque: the horizontal vorticity advection and the meridional gradient of the torque (contours and colored shading, respectively, in the left panel) and the vertical advection and twisting term defined as $-\mathbf{k}\cdot\nabla\times(\omega\partial\mathbf{u}/\partial p)$ [see (7) in Sardeshmukh and Held 1984)] (right panel). In the presence of midlatitude baroclinicity (top), the balance in the vicinity of the torque is similar to that in (5). However, to the west, the vertical advection and twisting term is large and in balance with the horizontal advection term. The vertical advection and twisting response is dominated by time-mean dynamics (not shown) and is mainly due to change in vertical shear of the horizontal flow. Poleward of 10° the horizontal advection term is largely in balance with the stretching term (not shown). Note that the vorticity balance in the presence of baroclinicity is largely nonlinear in contrast to (5) and (8). In the absence of baroclinicity (bottom),

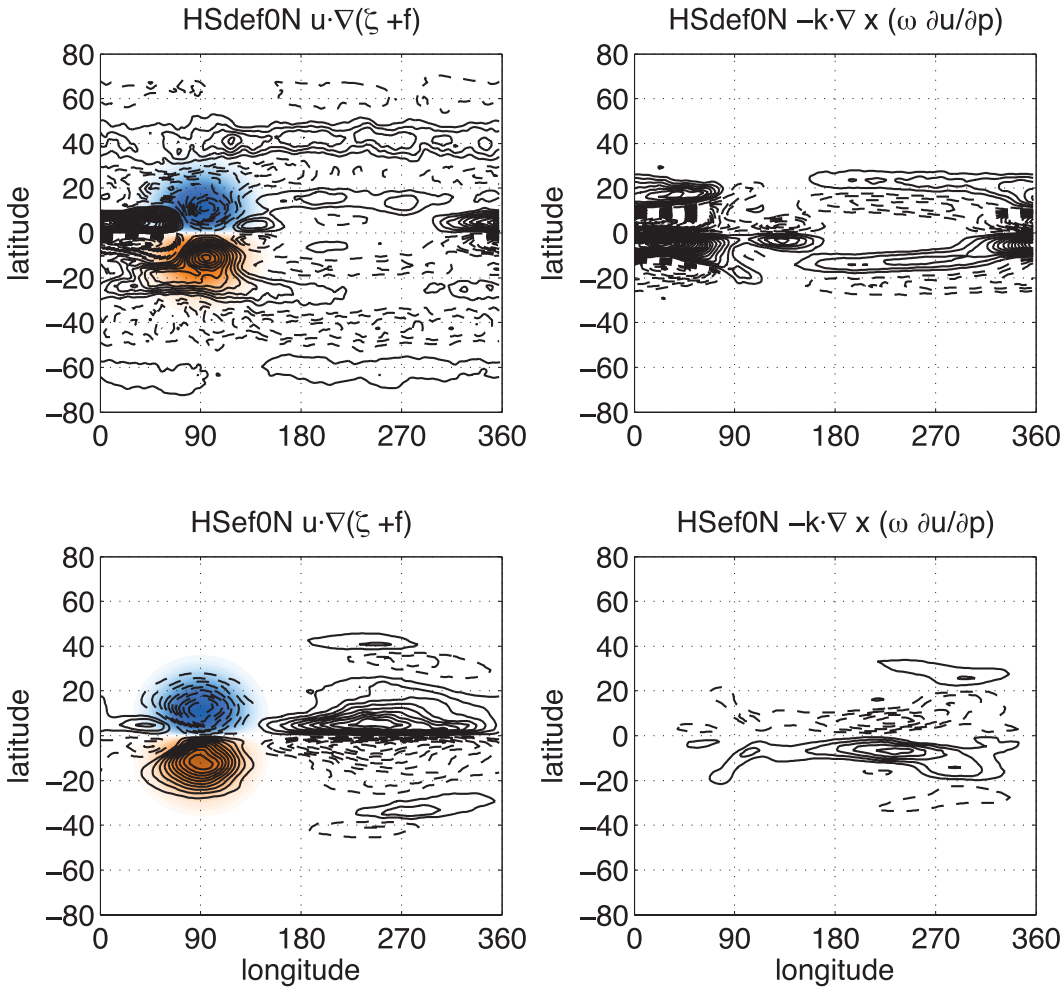

FIG. 11. The nonlinear GCM vorticity budget response to the single-signed equatorial torque at 142 hPa for the HS94 configuration in the (top) presence and (bottom) absence of basic-state baroclinicity. (left) Horizontal vorticity advection and meridional gradient of the torque (contours and shading, respectively) terms. (right) Vertical advection and twisting term. CI is 1×10^{-11} s^{-1}.

the dominant balance is similar to that in the N06 configuration (see Fig. 5) in the vicinity of the torque. The additional horizontal advection contribution to the east of the torque is associated with transient HEMFC (as discussed below) and is not as large in the N06 configuration response because it includes free-tropospheric Rayleigh drag. Also, because there is no horizontal flow in the basic state in the absence of baroclinicity, the changes in the vertical advection and twisting term are much smaller.

The changes in the vorticity budget in the presence of midlatitude baroclinicity, and more generally the entire extratropical response, can be understood from changes in the HEMFC. At upper levels HEMFC plays an important role in the general circulation in midlatitudes (Held 2000). It is primarily balanced by the Coriolis torque and therefore contributes to the structure of the Ferrel cell. Figure 12 shows the anomalous transient HEMFC at 142 hPa (defined as the deviation from the time average only; left) and the zonal-mean HEMFC response (right) to a zonally asymmetric equatorial torque for the HS94 configuration in the presence and absence of basic state baroclinicity (top and bottom, respectively). The response in the presence of baroclinicity (top) involves upper-level equatorial HEMFC, which is confined to the region of the torque and to the west. This equatorial HEMFC is suggestive of a region of equatorial Rossby wave emission[4] and is also seen in response to an imposed midlevel diabatic heating (see N06's Fig. 7b). The linear Gill model

[4] An analysis of daily mean horizontal and vertical winds revealed westward-propagating wind anomalies with horizontal structures consistent with those of equatorial Rossby waves (not shown).

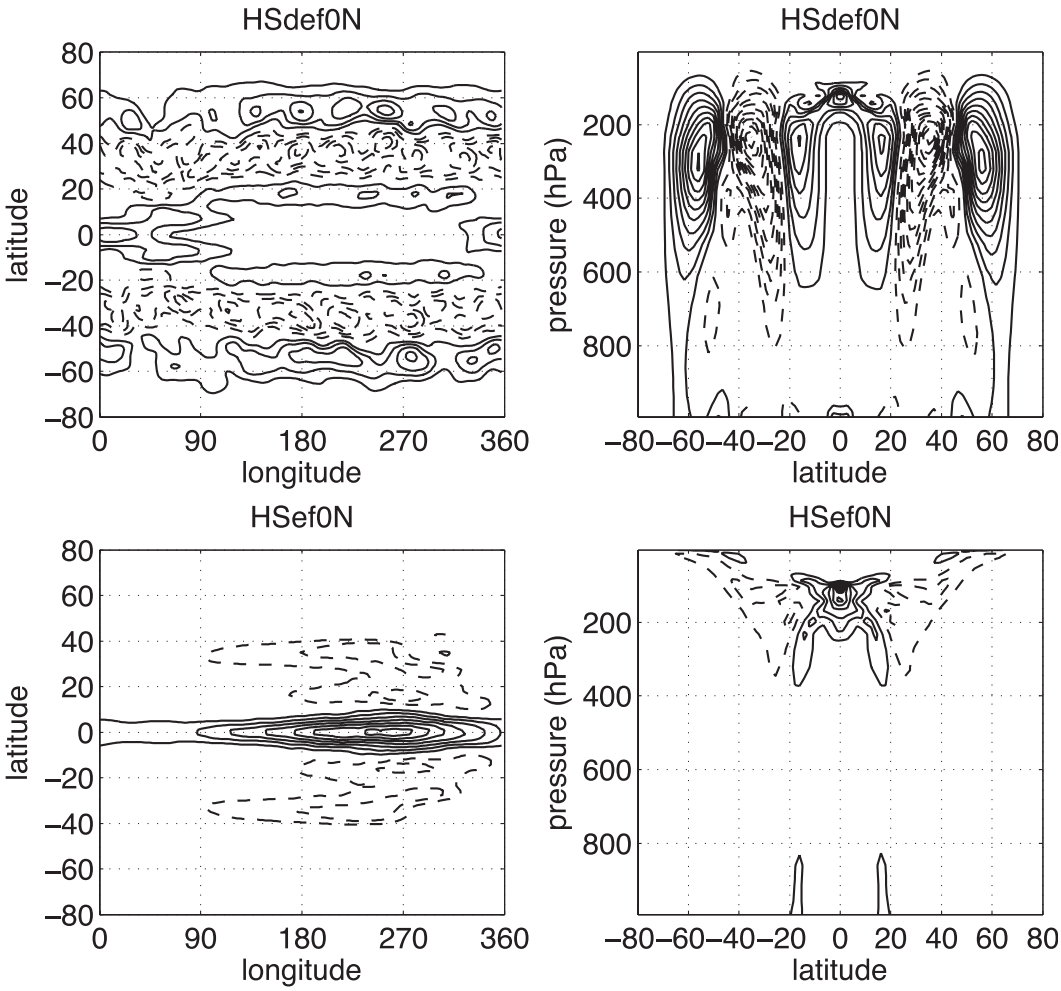

FIG. 12. The nonlinear GCM horizontal eddy momentum flux convergence response to the $\mathcal{F}0$ torque at 142 hPa for the HS94 configuration in the (top) presence and (bottom) absence of basic-state baroclinicity. (left) Transient HEMFC response. (right) Zonal-mean HEMFC response. Top panels are the anomaly relative to the basic state (shown in right panel of Fig. 8). CI is (left) 0.5 and (right) 0.25 m s^{-1} day^{-1}.

zonal wind response to a unit torque satisfies a necessary criterion (Kuo 1949) for barotropic instability (not shown). To the east of the torque and poleward of 10°, the HEMFC is nearly zonally symmetric and corresponds to a poleward shift of the basic-state zonal-mean HEMFC. Therefore, there are two different HEMFC responses: a tropical response associated with equatorial Rossby waves, which occurs above 200 hPa, and the poleward shift of the baroclinic HEMFC in midlatitudes. The pattern in midlatitudes, when balanced by the Coriolis torque, drives a meridional flow response in the upper troposphere in the steady limit, which is consistent with the streamfunction response shown in Fig. 9 (top right). Note that the HEMFC responses are consistent with the horizontal vorticity advection response at 142 hPa, which is balanced by the stretching term response in the vorticity budget. In the absence of basic-state baroclinicity (bottom) there is a clear equatorial HEMFC response associated with equatorial Rossby waves; however, it occurs to the east of the torque, which is likely the result of a lack of basic-state horizontal flow. There is also a subtropical divergence that extends into the stratosphere; however, there is no response in midlatitudes, consistent with the vorticity budget.

Randel and Held (1991) showed that regions of baroclinic HEMFC in the upper troposphere are confined by the critical surface for midlatitude baroclinic eddies, namely where the eddy phase speed equals the zonal-mean zonal wind speed. This suggests that if the zonal-mean zonal wind in the upper troposphere were to change because of an external forcing, the HEMFC would shift in response, all else being equal. A zonally asymmetric equatorial torque was shown to significantly impact the zonal-mean zonal wind in the upper troposphere (see

Fig. 4), suggesting a possible cause for the poleward shift of the baroclinic HEMFC. Figure 13 shows the HEMFC phase speed spectra response to a zonally asymmetric torque at (top) 0°, (middle) 10°, and (bottom) 30°N at 273 hPa, which is the level where the HEMFC peaks in midlatitudes (see Fig. 12, top left). The colored shading shows the phase speed spectra in the absence of the torque and the thin contours show the spectra in the presence of the torque. The thick solid line shows the zonal-mean zonal wind in the presence of the torque. When the torque is placed at the equator, the zonal-mean zonal wind and the HEMFC shift poleward by over 5° (top). The zonal wind response in the presence of the torque is close to being equal to the basic-state zonal wind plus the zonal wind response to the torque in the absence of midlatitude baroclinic eddies (thick dashed line), which suggests that the baroclinic eddies are responding to the torque-induced changes in zonal wind (i.e., changes in the position of the critical line). This is also confirmed by the relatively small changes in the structure of the HEMFC, which to leading order simply shifts poleward. The shift in HEMFC is consistent with the anomalous streamfunction response, which in the midlatitudes consists of a poleward shift of the basic-state streamfunction [cf. Fig. 9 (top right) and Fig. 8 (left)]. As the torque is moved to 10°N, both the zonal-mean zonal wind and the HEMFC shift farther poleward (Fig. 13, middle). The changes in structure of the HEMFC are once again relatively small. Finally when the torque is placed at 30°N (Fig. 13, bottom) it overlaps with the region of zero HEMFC and the HEMFC does not shift significantly but does change in structure. In this case, the torque reduces the magnitude of the eastward wind in the extratropics and thus does not affect the phase speeds of the slower eddies and does not lead to a jet shift.

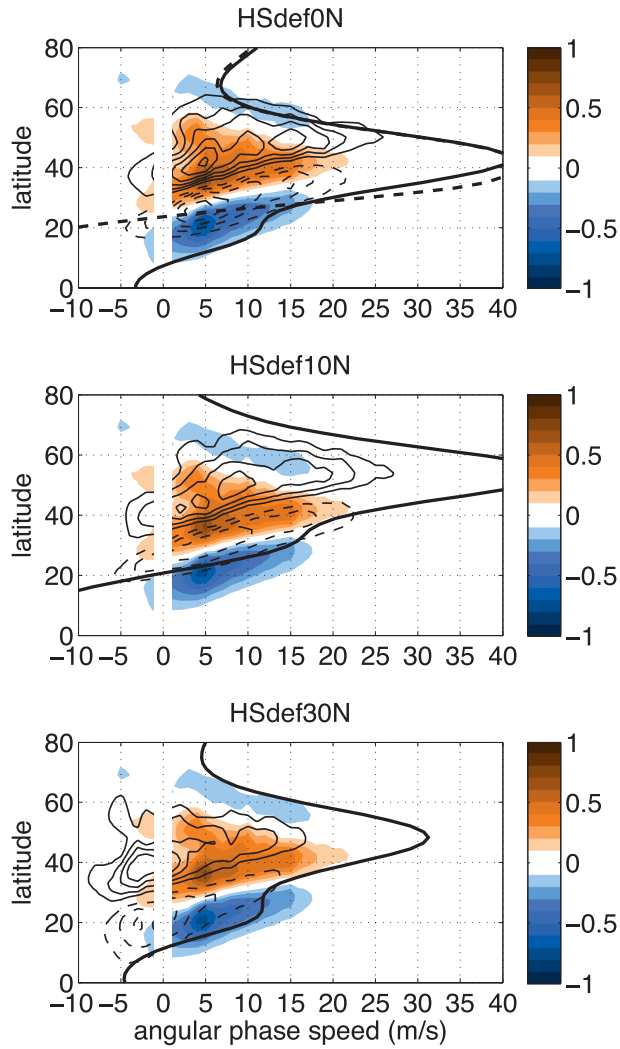

FIG. 13. Phase speed spectra vs latitude of the HEMFC at 273 hPa in the basic state (shading) and the response (contours; showing total and not anomalies) to the single-signed torques placed at (top) 0°, (middle) 10°, and (bottom) 30°N for the HS94 configuration. CI is 0.5 m s^{-1} day^{-1}. The zonal-mean (angular) zonal wind response to the torques is shown as a thick solid line, and in the top panel the thick dashed line shows the sum of the basic-state zonal-mean zonal wind and the zonal-mean zonal wind response to the single-signed equatorial torque in the absence of basic-state baroclinicity.

4. Summary and discussion

We have examined the tropospheric response to prescribed zonally asymmetric tropical and subtropical torques, which can be considered as idealizations of vertical momentum flux convergence due to orographic gravity waves or convection. The linear analytical and nonlinear numerical responses to the prescribed torques were considered. The response in the presence and in the absence of midlatitude baroclinicity was also explored.

The linear analytic response to a zonally asymmetric torque was found by forcing the canonical Gill (1980) model with a prescribed torque. The horizontal structure of the response to a zonally asymmetric upper-level equatorial westward torque is significantly different from the response to a midlevel equatorial diabatic heating. There is weak vertical motion in the vicinity of the torque and strong upwelling in the vicinity of the heating. To the east of the respective forcing, both responses project onto a Kelvin wave pattern; however, the projection is of the opposite sign. Consequently, to the east of the torque at upper levels there is westward flow and to the east of the heating there is eastward flow. This difference in the sign of the response to the east suggests that in situations where both forcings are present the responses may destructively interfere. To the west of the forcing, however, both responses project onto a Rossby wave pattern of the same sign. The zonal-mean streamfunction response to the equatorial

forcings is identical for an identical forcing amplitude, with both responses producing equatorial upwelling with Hadley-type cells on either side of the equator. The zonal-mean zonal wind response to the torque is in balance with the meridional gradient of the geopotential height, whereas the zonal wind response to the heating is consistent with planetary vorticity advection by the mean Hadley cell flow. When the torque and heating are shifted into the NH tropics, the NH response to the equatorial forcing is strengthened while the SH response weakens. In this case the difference between the horizontal flow response to the two forcings is similar to the difference seen for the equatorial forcings. In contrast, the zonal-mean streamfunction responses are completely opposite, with upwelling in the SH in response to the off-equatorial torque and upwelling in the NH in response to the off-equatorial heating.

The nonlinear response to zonally asymmetric torques was explored in idealized GCM simulations. The response was considered for basic states with and without large-scale meridional temperature gradients. The nonlinear response to a prescribed equatorial baroclinic torque was in qualitative agreement with the Gill (1980) model response for the same model set up (i.e., with Rayleigh drag throughout the atmosphere). The flow at the equator was more zonally symmetric than the Gill model response. The addition of nonlinear terms did not significantly alter the zonal-mean responses. However, the Hadley cell responses in the idealized GCM simulations are about an order of magnitude weaker than the observed annual mean Hadley cell. The strength of the response will likely change considerably with the addition of moist processes.

An upper-level vorticity budget analysis revealed that planetary vorticity advection balances the meridional gradient of the zonally asymmetric equatorial torque. In contrast, the equatorial heating response involves the balance of planetary vorticity advection and the stretching term. These differences can be used to explain the different zonal-mean upwelling patterns. The zonal-mean upwelling response to the heating is balanced directly by the heating according to a weak-temperature gradient balance (Sobel and Bretherton 2000). In contrast, the zonal-mean meridional wind response is in balance with the meridional gradient of the torque, which is analogous to a downward control–type balance (Haynes et al. 1991), and the zonal-mean upwelling response follows from the continuity equation. An upper-level divergence budget analysis revealed that the meridional momentum contribution to the divergence balance was in geostrophic balance while the zonal momentum contribution involved a balance between the second derivative of the geopotential height and the zonal gradient of the torque. The vorticity and divergence balances can be combined to infer the divergent wind response and raise the possibility of using the linear steady-state balanced equations to obtain a balanced response to the torque.

The torque was subsequently imposed principally at upper levels and moved into the subtropics to mimic the vertical momentum flux convergence associated with orographic gravity waves excited by, for example, an extratropical westerly jet interacting with a mountain range. When the upper-level torque was placed at the equator and 10°N the responses were similar to the linear and nonlinear responses to the equivalent baroclinic torque. The zonal-mean streamfunction response to the torque is consistent with the mean meridional circulation induced by the westward phase of the quasi-biennial oscillation in the stratosphere (Plumb and Bell 1982). When the torque was placed at the edge of the subtropics (at 30°N), the vertical velocity response became zonally confined with downwelling to the northeast and upwelling to the southwest. The vorticity balance response to this torque involved planetary vorticity advection, vortex stretching, and the meridional gradient of the torque. In the zonal mean this vorticity balance is similar to a downward control balance (Haynes et al. 1991) and leads to a mean meridional circulation extending from the torque to the surface.

Midlatitude baroclinic eddies significantly modified the response to the prescribed zonally asymmetric torque. When the torque was placed at the equator or 10°N, the response involved a Walker-type circulation just north of 20°N and zonally symmetric downwelling and upwelling from 30° to 60°N. The streamfunction response involved the extension of the direct Hadley circulation into midlatitudes and the Ferrel cell toward the pole. An analysis of the vorticity budget in the upper troposphere revealed that in the presence of midlatitude baroclinic eddies the balance in response to an equatorial torque was similar to that in the absence of a meridional temperature gradient only in the vicinity of the torque. Away from the torque the balance was no longer linear. To the west, the response involved a balance among horizontal vorticity advection, vertical advection, and twisting and stretching terms, whereas to the east of the torque and poleward of 10° the response involved a balance between the horizontal advection and stretching terms. The vorticity balance to the west reflects the emission of equatorial Rossby waves in response to the equatorial torque and is likely due to the barotropically unstable nature of the zonal wind response. Elsewhere the vorticity budget is consistent with a balance between the Coriolis torque and the baroclinic HEMFC, which shifts poleward in response to an equatorial torque.

The circulation response in midlatitudes was consistent with the poleward shift of the HEMFC. The shift in

the HEMFC coincided with a poleward shift of the eddy critical line, which was induced by the zonal wind response to the imposed torque, providing a possible cause for the changes in midlatitudes below 200 hPa. Previous authors have noted similar shifts in the regions of HEMFC (Chen and Zurita-Gotor 2008) and the tropospheric jet (Ring and Plumb 2007; Chen and Zurita-Gotor 2008; Garfinkel and Hartmann 2011) in response to zonally symmetric torques in the tropical and subtropical upper troposphere and lower stratosphere. They found a significant eddy-induced response when the response to the torque overlapped with the northern annular mode in their respective idealized GCMs. However, the poleward shift found in the present results might also occur for a different reason (e.g., changes in the eddy phase speed or length scale). Interestingly the magnitude of the poleward shift of the jet and regions of HEMFC in response to zonally asymmetric torques in the present results were similar for zonally symmetric torques of identical amplitude (not shown), suggesting that baroclinic eddies respond primarily to the zonal-mean effects of the torque.

The present results have isolated the linear analytical and nonlinear numerical tropospheric responses to prescribed zonally asymmetric torques in the tropics and subtropics. The idealized GCM responses suggest that torques at 0° and 10°N impact the tropical Hadley cell and the zonal structure of upwelling and downwelling, and thus the intertropical convergence zones and possibly also the Walker circulation. These impacts are consistent with recent studies that have shown that including CMT in fully comprehensive GCMs impacts the modeled Hadley and Walker circulations (Zhang and McFarlane 1995; Wu et al. 2003, 2007; Richter and Rasch 2008). Similarly, the idealized GCM response to a torque at 30°N leads to weakened zonal winds in the NH and a weakened Ferrel cell, which is consistent with studies that have highlighted the impact of OGWD in the troposphere in GCMs during NH winter (Palmer et al. 1986; McFarlane 1987; Stephenson 1994; Chen and Zurita-Gotor 2008). Note however that most of the previously mentioned studies focused on the zonal-mean impacts whereas the present results have isolated the zonally asymmetric structure of the response, which involves significantly downwelling to the northeast of the 30°N torque. The dominant vorticity and divergence balances in the vicinity of the torques suggest the possibility of obtaining a balanced response, which could be used to isolate dynamically induced vertical motion from that associated with other processes such as moist convection. We will report on this in a future study. Since we have assessed the impacts in an idealized context there are a number of open questions. For example, in the real atmosphere—which includes moist processes, exhibits significant zonal asymmetries in its lower boundary conditions, has torques with significant intermittency in time, and allows for feedbacks between the torque and the large-scale circulation— how is the response modified? Understanding the impact of more realistic configurations on the response is the subject of future investigation.

Acknowledgments. TAS acknowledges support from the Natural Sciences and Engineering Research Council of Canada through a postdoctoral fellowship. WRB began this work while supported by the John and Elaine French Environmental Fellowship and the Reginald A. Daly Postdoctoral Fellowship in the Department of Earth and Planetary Sciences at Harvard University. This work was supported in part by the facilities and staff of the Yale University Faculty of Arts and Sciences High Performance Computing Center, and by the National Science Foundation under Grant CNS 08-21132 that partially funded acquisition of the facilities. The authors are grateful to two anonymous reviewers for their helpful comments.

APPENDIX

Gill Model Solution to a Prescribed Torque

The Gill (1980) model solution to a prescribed torque $\mathcal{F}$ can be obtained by setting $Q = 0$ and adding $\mathcal{F}$ to the right-hand side of (2.6) in Gill (1980). The addition of the torque changes (2.10) in Gill to

$$\epsilon^3 v + \frac{1}{4}\epsilon y^2 v - \epsilon\frac{\partial^2 v}{\partial x^2} - \epsilon\frac{\partial^2 v}{\partial y^2} - \frac{1}{2}\frac{\partial v}{\partial x} = \frac{\partial^2 \mathcal{F}}{\partial x \partial y} - \frac{1}{2}\epsilon y \mathcal{F}. \tag{A1}$$

Upon changing variables to $q = p + u$ and $r = p - u$, we obtain

$$\epsilon q + \frac{\partial q}{\partial x} + \frac{\partial v}{\partial y} - \frac{1}{2}yv = \mathcal{F}, \tag{A2a}$$

$$\epsilon r - \frac{\partial r}{\partial x} + \frac{\partial v}{\partial y} + \frac{1}{2}yv = -\mathcal{F}, \tag{A2b}$$

$$\frac{\partial q}{\partial y} + \frac{1}{2}yq + \frac{\partial r}{\partial y} - \frac{1}{2}yr = 0. \tag{A2c}$$

All functions are subsequently expanded into parabolic cylinder functions $D_n(y)$ [e.g., $q = \sum_{n=0}^{\infty} q_n(x) D_n(y)$], such that

$$\epsilon q_0 + \frac{dq_0}{dx} = \mathcal{F}_0,$$

$$\epsilon q_{n+1} + \frac{dq_{n+1}}{dx} - v_n = \mathcal{F}_{n+1} \quad n \geq 0, \tag{A3a}$$

$$\epsilon r_{n-1} - \frac{dr_{n-1}}{dx} + nv_n = -\mathcal{F}_{n-1} \quad n \geq 1, \tag{A3b}$$

$$q_1 = 0$$

$$r_{n-1} = (n+1)q_{n+1} \quad n \geq 1. \tag{A3c}$$

Note that (A3) is similar to (3.9)–(3.11) in Gill (1980).

a. Response to a hemispherically symmetric torque

If the torque is symmetric about the equator, as when

$$F = F_0 \exp\left(-\frac{1}{4}y^2\right) = -\cos(kx)\exp\left(-\frac{1}{4}y^2\right), \tag{A4}$$

the response involves two parts, as for the response to a symmetric diabatic heating. The first part is the Kelvin wave response and is found by taking $n = 0$; for example,

$$(\epsilon^2 + k^2)q_0 = \begin{cases} 0 & \text{for} \quad x < -L, \\ -\epsilon\cos(kx) - k\{\sin(kx) + \exp[-\epsilon(x+L)]\} & \text{for} \quad |x| < L, \\ -k[1 + \exp(-2\epsilon L)]\exp[\epsilon(L - x)] & \text{for} \quad x > L. \end{cases} \tag{A5}$$

Note that the Kelvin wave part of the response to the symmetric torque at upper levels is identical to that for the symmetric diabatic heating at lower levels [see (4.2) in Gill (1980)]. This is because Q_0 is similar to $-F_0$.

The second part of the response corresponds to a long planetary wave, which is the solution to (A3) for $n = 1$, that is,

$$\frac{dq_2}{dx} - 3\epsilon q_2 = F_0. \tag{A6}$$

The solution is

$$[(2n+1)^2\epsilon^2 + k^2]q_{n+1} = \begin{cases} k\{1 + \exp[-2(2n+1)\epsilon L]\exp[(2n+1)\epsilon(x+L)]\} & \text{for} \quad x < -L, \\ (2n+1)\epsilon\cos(kx) - k\{\sin(kx) - \exp[(2n+1)\epsilon(x-L)]\} & \text{for} \quad |x| < L, \\ 0 & \text{for} \quad x > L. \end{cases} \tag{A7}$$

The velocity and pressure responses are

$$p = \frac{1}{2}q_0(x)\exp\left(-\frac{1}{4}y^2\right) + \frac{1}{2}q_2(1 + y^2)\exp\left(-\frac{1}{4}y^2\right), \tag{A8a}$$

$$u = \frac{1}{2}q_0(x)\exp\left(-\frac{1}{4}y^2\right) + \frac{1}{2}q_2(y^2 - 3)\exp\left(-\frac{1}{4}y^2\right), \tag{A8b}$$

$$v = (F_0 y + 4\epsilon q_2 y)\exp\left(-\frac{1}{4}y^2\right), \tag{A8c}$$

$$w = -\frac{1}{2}\epsilon q_0(x)\exp\left(-\frac{1}{4}y^2\right) - \frac{1}{2}\epsilon q_2(1 + y^2)\exp\left(-\frac{1}{4}y^2\right), \tag{A8d}$$

and they are plotted in Fig. 2 (bottom), with $k = \pi/2L$.

b. Response to a hemispherically symmetric plus asymmetric torque

If the torque is the sum of a symmetric and asymmetric torque, say

$$F = F_0 + F_1 = -[\cos(kx) + y\cos(kx)]\exp\left(-\frac{1}{4}y^2\right), \tag{A9}$$

then the response can be considered as the linear combination of the individual responses. The response to the symmetric torque is identical to (A8). The asymmetric response can be considered as two parts. The first part corresponds to a $n = 0$ mixed planetary–gravity wave with

$$q_1 = 0, \quad v_0 = F_1. \tag{A10}$$

Note that the response is zero outside the forcing region.

The second part of the response corresponds to a long planetary wave, which is the solution to (A3) for $n = 2$; that is,

$$\frac{dq_3}{dx} - 5\epsilon q_3 = F_1. \tag{A11}$$

The solution is (A7) for $n = 2$. The velocity and pressure responses to the asymmetric torque are

$$p_{\text{asym}} = \frac{1}{2}q_3(x)y^3 \exp\left(-\frac{1}{4}y^2\right), \tag{A12a}$$

$$u_{\text{asym}} = \frac{1}{2}q_3(x)(y^3 - 6y)\exp\left(-\frac{1}{4}y^2\right), \tag{A12b}$$

$$v_{\text{asym}} = [6\epsilon q_3(y^2 - 1) + F_0 y^2 - 2F_0]\exp\left(-\frac{1}{4}y^2\right), \tag{A12c}$$

$$w_{\text{asym}} = -\frac{1}{2}\epsilon q_3(x)y^3 \exp\left(-\frac{1}{4}y^2\right). \tag{A12d}$$

The total response is the sum of (A12) and (A8) and is plotted in Fig. 3 (bottom).

REFERENCES

Andrews, D. G., J. R. Holton, and C. B. Leovy, 1987: *Middle Atmosphere Dynamics*. Academic Press, 489 pp.

Bordoni, S., and T. Schneider, 2008: Monsoons as eddy-mediated regime transitions of the tropical overturning circulation. *Nat. Geosci.,* **1,** 515–519.

Carr, M. T., and C. S. Bretherton, 2001: Convective momentum transport over the tropical Pacific: Budget estimates. *J. Atmos. Sci.,* **58,** 1673–1693.

Chen, G., and P. Zurita-Gotor, 2008: The tropospheric jet response to prescribed zonal forcing in an idealized atmospheric model. *J. Atmos. Sci.,* **65,** 2254–2271.

Eliassen, A., 1951: Slow thermally or frictionally controlled meridional circulation in a circular vortex. *Astrophys. Norv.,* **5,** 19–60.

Garfinkel, C. I., and D. L. Hartmann, 2011: The influence of the quasi-biennial oscillation on the troposphere in wintertime in a hierarchy of models. Part I: Simplified dry GCMs. *J. Atmos. Sci.,* **68,** 1273–1289.

Gill, A. E., 1980: Some simple solutions for heat-induced tropical circulation. *Quart. J. Roy. Meteor. Soc.,* **106,** 447–462.

Gregory, D., R. Kershaw, and P. M. Inness, 1997: Parameterization of momentum transport by convection. II: Tests in single column and general circulation models. *Quart. J. Roy. Meteor. Soc.,* **123,** 1153–1183.

Haynes, P. H., C. J. Marks, M. E. McIntyre, T. G. Shepherd, and K. P. Shine, 1991: On the "downward control" of extratropical diabatic circulations by eddy-induced mean zonal forces. *J. Atmos. Sci.,* **48,** 651–678.

Held, I. M., 2000: The general circulation of the atmosphere. *Proc. 2000 Program in Geophysical Fluid Dynamics,* Woods Hole, MA, WHOI. [Available online at http://www.whoi.edu/page.do?pid=13076.]

——, and A. Y. Hou, 1980: Nonlinear axially symmetric circulations in a nearly inviscid atmosphere. *J. Atmos. Sci.,* **37,** 515–533.

——, and M. J. Suarez, 1994: A proposal for the intercomparison of the dynamical cores of atmospheric general circulation models. *Bull. Amer. Meteor. Soc.,* **75,** 1825–1830.

Holton, J. R., P. H. Haynes, M. E. McIntyre, A. R. Douglass, R. B. Rood, and L. Pfister, 1995: Stratosphere–troposphere exchange. *Rev. Geophys.,* **33,** 403–439.

Kuo, H., 1949: Dynamic instability of two-dimensional nondivergent flow in a barotropic atmosphere. *J. Meteor.,* **6,** 105–122.

LeMone, M. A., 1983: Momentum transport by a line of cumulonimbus. *J. Atmos. Sci.,* **40,** 1815–1834.

——, G. M. Barnes, and E. J. Zipser, 1984: Momentum flux by lines of cumulonimbus over the tropical ocean. *J. Atmos. Sci.,* **41,** 1914–1932.

Lilly, D., and P. Kennedy, 1973: Observations of a stationary mountain wave and its associated momentum flux and energy dissipation. *J. Atmos. Sci.,* **30,** 1135–1152.

Lin, J.-L., M. Zhang, and B. Mapes, 2004: Zonal momentum budget of the Madden–Julian oscillation: The source and strength of equivalent linear damping. *J. Atmos. Sci.,* **62,** 2172–2188.

Matsuno, T., 1966: Quasi-geostrophic motions in the equatorial area. *J. Meteor. Soc. Japan,* **44,** 25–43.

McFarlane, N. A., 1987: The effect of orographically excited gravity-wave drag on the circulation of the lower stratosphere and troposphere. *J. Atmos. Sci.,* **44,** 1775–1800.

Neale, R., and Coauthors, 2010: Description of the NCAR Community Atmosphere Model (CAM 5.0). NCAR Tech. Rep. NCAR/TN-486+STR, 282 pp.

Neelin, J., 1989: On the interpretation of the Gill model. *J. Atmos. Sci.,* **46,** 2466–2468.

——, and I. Held, 1987: Modeling tropical convergence based on the moist static energy budget. *Mon. Wea. Rev.,* **115,** 3–12.

Norton, W. A., 2006: Tropical wave driving of the annual cycle in tropical tropopause temperatures. Part II: Model results. *J. Atmos. Sci.,* **63,** 1420–1431.

Palmer, T. N., G. J. Schutts, and R. Swinbank, 1986: Alleviation of a systematic westerly bias in general circulation and numerical weather prediction models through an orographic gravity wave drag parameterization. *Quart. J. Roy. Meteor. Soc.,* **112,** 1001–1039.

Plumb, R. A., and R. C. Bell, 1982: A model of the quasi-biennial oscillation on an equatorial beta-plane. *Quart. J. Roy. Meteor. Soc.,* **108,** 335–352.

Randel, W. J., and I. M. Held, 1991: Phase speed spectra of transient eddy fluxes and critical layer absorption. *J. Atmos. Sci.,* **48,** 688–697.

Richter, J. H., and P. J. Rasch, 2008: Effects of convective momentum transport on the atmospheric circulation in the Community Atmosphere Model, version 3. *J. Climate,* **21,** 1487–1499.

Ring, M. J., and R. A. Plumb, 2007: Forced annular mode patterns in a simple atmospheric general circulation model. *J. Atmos. Sci.,* **64,** 3611–3626.

Sardeshmukh, P. D., and I. M. Held, 1984: The vorticity balance in the tropical upper troposphere of a general circulation model. *J. Atmos. Sci.,* **41,** 768–778.

Schneider, E. K., and R. S. Lindzen, 1976: A discussion of the parameterization of momentum exchange by cumulus convection. *J. Geophys. Res.,* **81,** 3158–3160.

Schneider, T., and S. Bordoni, 2008: Eddy-mediated regime transitions in the seasonal cycle of a Hadley circulation and implications for monsoon dynamics. *J. Atmos. Sci.,* **65,** 915–934.

Shepherd, T. G., K. Semeniuk, and J. N. Koshyk, 1996: Sponge layer feedbacks in middle-atmosphere models. *J. Geophys. Res.,* **101,** 23 447–23 464.

Sobel, A. H., and C. S. Bretherton, 2000: Modeling tropical precipitation in a single column. *J. Climate,* **13,** 4378–4392.

——, J. Nilsson, and L. M. Polvani, 2001: The weak temperature gradient approximation and balanced tropical moisture waves. *J. Climate,* **58,** 3650–3665.

Song, X., X. Wu, G. J. Zhang, and R. W. Arritt, 2008: Dynamical effects of convective momentum transports on global climate simulations. *J. Climate,* **21,** 180–194.

Song, Y., and W. A. Robinson, 2004: Dynamical mechanisms for stratospheric influence on the troposphere. *J. Atmos. Sci.,* **61,** 1711–1725.

Stephenson, D. B., 1994: The Northern Hemisphere tropospheric response to changes in the gravity-wave drag scheme in a perpetual January GCM. *Quart. J. Roy. Meteor. Soc.,* **120,** 699–712.

Stevens, D. E., 1979: Vorticity, momentum and divergence budgets of synoptic-scale wave disturbances in the tropical eastern Atlantic. *Mon. Wea. Rev.,* **107,** 535–550.

Thompson, D., and J. Wallace, 2000: Annular modes in the extratropical circulation. Part I: Month-to-month variability. *J. Climate,* **13,** 1000–1016.

Walker, C. C., and T. Schneider, 2006: Eddy influences on Hadley circulations: Simulations with an idealized GCM. *J. Atmos. Sci.,* **63,** 3333–3350.

Wu, X., X.-Z. Liang, and G. J. Zhang, 2003: Seasonal migration of ITCZ precipitation across the equator: Why can't GCMs simulate it? *Geophys. Res. Lett.,* **30,** 1824, doi:10.1029/2003GL017198.

——, L. Deng, X. Song, G. Vettoretti, W. R. Peltier, and G. J. Zhang, 2007: Impact of a modified convective scheme on the Madden–Julian oscillation and El Niño–Southern Oscillation in a coupled climate model. *Geophys. Res. Lett.,* **34,** L16823, doi:10.1029/2007GL030637.

Zebiak, S., 1982: A simple atmospheric model of relevance to El Niño. *J. Atmos. Sci.,* **39,** 2017–2027.

Zhang, G. J., and H.-R. Cho, 1991: Parameterization of the vertical transport of momentum by cumulus clouds. Part I: Theory. *J. Atmos. Sci.,* **48,** 1483–1492.

——, and N. A. McFarlane, 1995: Role of convective-scale momentum transport in climate simulation. *J. Geophys. Res.,* **100,** 1417–1426.